NTNU
Kunnskap for en bedre verden

DEPARTMENT OF ELECTRONIC SYSTEMS

TFE4930 - MASTER THESIS

Multipath channel estimation between two nodes using Multi Carrier Phase Difference (MCPD)

Author:
Ruben Hendrickx

Supervisor:
Prof. dr. ir. Jo Verhaevert
Prof. dr. Torbjörn Ekman

Co-supervisor:
Carsten Wulff

June, 2023

Abstract

Keywords: Multi Carrier Phase Difference — Multipath channel — Radio Frequency — Least squares estimation

This thesis focuses on the possibility of a multipath channel to be estimated. How it can be estimated and if the estimation results in an accurate representation of the true multipath channel. The research starts by describing the purpose of this study and establishing the boundaries within this thesis. Afterwards, two theoretical models are proposed and a method for analyzing these models. Following this, the proposed theoretical models were tested. The results conclude that it is possible to estimate the multipath channel. However, the theoretical model needs to match with the hardware used in practice. The conclusion reflects on the research and suggests improvements for the theoretical model.

Multipath channel estimation between two nodes using Multi Carrier Phase Difference (MCPD)

Ruben Hendrickx, Norwegian University of Science and Technology (Rubhendr.hendrickx@UGent.be)

Supervisor(s): Prof. dr. Torbjörn Ekman, Prof. dr. ir. Jo Verhaevert

***Abstract* — This thesis focuses on the possibility of a multipath channel to be estimated. How it can be estimated and if the estimation results in an accurate representation of the true multipath channel. The research starts by describing the purpose of this study and establishing the boundaries within this thesis. Afterwards, two theoretical models are proposed and a method for analyzing these models. Following this, the proposed theoretical models were tested. The results conclude that it is possible to estimate the multipath channel. However, the theoretical model needs to match with the hardware used in practice. The conclusion reflects on the research and suggests improvements for the theoretical model.**

***Keywords* — Multi Carrier Phase Difference, Multipath channel, Radio Frequency, Least squares estimation**

I. Introduction

This thesis focusses on the possibility of a multipath channel to be estimated. This is researched by trying to answer two questions. How can a multipath channel be estimated and if the estimation results in an accurate representation of the true multipath channel.

If the multipath channel between a great amount of antennas can be estimated and analyzed, changes in the channel can be detected as well. These changes correspond to movements made by objects or people in the environment.

Since this thesis focusses on the possibility for the multipath channel to be estimated, only a simple setup is created. Figure 1 shows the setup for this thesis. Only two antennas and one reflecting object is used. Measurements were made in an anechoic chamber to ensure the multipath only consists of two paths.

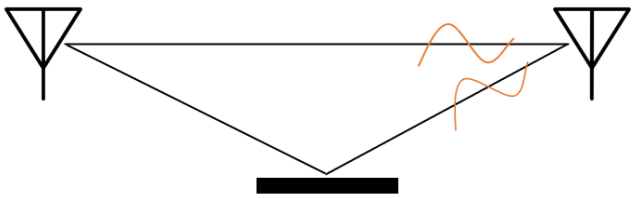

Figure 1: The general setup.

The antennas communicate with each other using MCPD. This is a ranging method [1][2] that returns accurate results even in multipath environments [3]. Research concerning MCPD evolves continuously[4][5], however most studies focus on the accuracy of this ranging method and on the robustness in different environmental situations.

In this thesis, it will be investigated if and how MCPD can be used to devise a theoretical model for the multipath channel. How can the theoretical model be analyzed and will it be an accurate representation of the true multipath channel.

To simulate and analyze the theoretical models, Matlab was used.

Being able to estimate the multipath channel allows for better movements sensors. This technology can also be implemented to map an environment. Some examples of practical utilization using this technology include better warehouse management, safety systems in nursing homes for elderly people and smarter intersection lights. These practical utilizations can contribute to the sustainable development goals [6].

II. Methodology

A. Multi Carrier Phase Difference (MCPD)

MCPD uses 40 frequency channels. The signals transmitted on these frequency channels will first travel from the first antenna (initiator) towards the second antenna (reflector). The reflector will then send the signals back to the initiator. At the initiator, the I and Q values corresponding to the channel can be measured.

This means that the channel is crossed twice, once in each direction. Taking into account the noise present, the transfer function available at the initiator given by the following equation:

$$G(f_k) = |H(f_k)|\, e^{i(2\phi_k + \epsilon_n)} + n_n$$

The phase ϕ_k can be isolated, divided by two and unwrapped. Multiplying this new phase with the magnitude |H|, results in the first presented theoretical model.

$$\hat{H}(f_k) = |G(f_k)|\, e^{i(\hat{\phi}_k)}$$

B. Least Squares Estimation (LSE)

To analyze this model, the LSE can be used. The frequencies corresponding to the frequency channels can be split into a carrier frequency and a multiple of the frequency step.

$$\sum_{n=1}^{N} a_n\, e^{(-i2\pi f_c \tau_n)}\, e^{(-i2\pi f_\Delta \tau_n k)}$$

R. Hendrickx is a master student at Ghent University (UGent), Gent, Belgium. This thesis was written abroad at Norwegian University of Science and Technology (NTNU), Trondheim, Norway.
E-mail: Rubhendr.hendrickx@UGent.be .

Now the equation can be simplified using the equations for c_n and ν_n, where n represents the different paths. The values for a_n and τ_n can be calculated from these variables.

From the value τ_n, the lengths of the different paths can be calculated.

$$c_n = a_n\, e^{(-i2\pi f_c \tau_n)}$$
$$\nu_n = 2\pi f_\Delta \tau_n$$

III. Simulation

Two situations were simulated. The first one has a LoS path length of 5m and a reflected path length of 15m. The second situation matches a realistic situation and has a LoS path length of 5.1m and a reflected path length of 6.1m. The theoretical magnitudes were set to 1 for the LoS path and 0.3 for the reflected path.

Table 1 shows the estimated path lengths for the first situation. The estimated lengths are really accurate for high SNR and lower in accuracy for smaller SNR values, which is to be expected.

Table 2 shows the estimated path lengths for the second situation. The estimated path length are still accurate for high SNR values. However, for lower SNR values the estimation becomes much more inaccurate.

Table 1: Path length estimations for a big path length difference for different SNR

SNR	LoS path [m]	Relative error [%]	Reflected path [m]	Relative error [%]
60 dB	5.0021	0.042	15.0014	0.0093
40 dB	4.9742	0.516	15.0920	0.613
20 dB	4.9589	0.822	16.1697	7.796

Table 2: Path length estimations for a small path length difference for different SNR

SNR	LoS path [m]	Relative error [%]	Reflected path [m]	Relative error [%]
60 dB	5.0777	0.446	6.0662	0.563
40 dB	5.2364	2.67	8.5534	40.2
20 dB	5.2675	2.75	/	/

Figures 2 and 3 show the path magnitude estimations for the different path in the first and second scenario in orange respectively. Normalizing these estimations is possible since only the ratio of reflected path magnitude to LoS path magnitude is important. However, these ratios do not match their expected values.

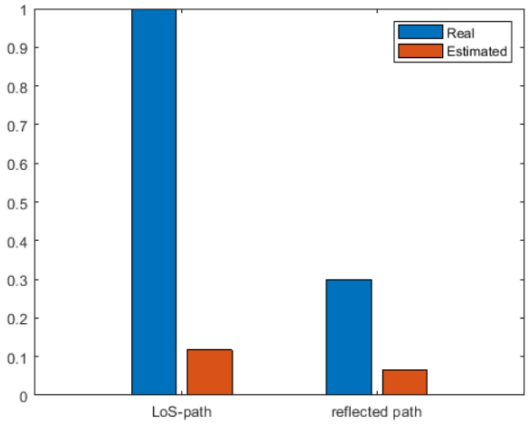

Figure 2: Estimated magnitudes compared with the real magnitudes for a big difference in path length.

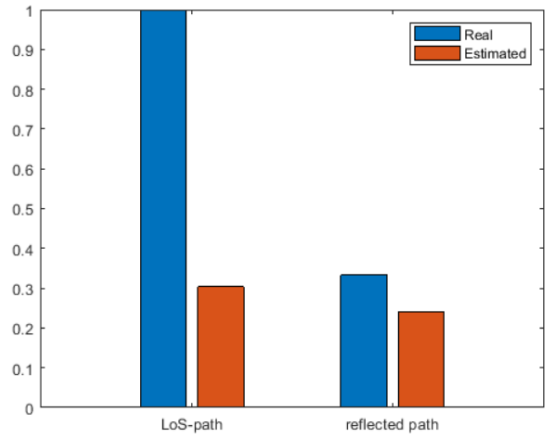

Figure 3: Estimated magnitudes compared with the real magnitudes for a small difference in path length.

IV. Measurements

The measurements were made in an anechoic chamber to ensure that only two and no extra paths were present in the multipath. Here measurements were made for three situations. The LoS path is always 5.1m long and the reflected path length varies for the different situations. They are 6.1m, 6.3m and 6.6m for situation 1, 2 and 3 respectively. Table 3 shows the results for these three situations after analyzing the measured transfer functions.

The magnitude estimations again do not match the expected ratio. The path length estimations match with half of the expected values.

Table 3: Results after analyzing the measured transfer functions

Situation	Type of path	Estimated length r [m]	Estimated magnitude ratio
1	LoS	2.5246	0.8651
	Reflected	3.4444	
2	LoS	2.5712	0.9565
	Reflected	3.6874	
3	LoS	2.6233	0.9262
	Reflected	3.8380	

Since the theoretical model does not match the measurements, a second version was devised.

V. Revision

A. New theoretical model

The measurement method deviates slightly from the traditional MCPD technology [7]. Instead of measuring the transfer function only once at the initiator, the I and Q values are measured once at the initiator and once at the reflector. Two transfer functions can be established using these I and Q values. In both, there is an extra phase shift present due to the phase difference between the initiator's and reflector's Local Oscillators.

$$X_i + jY_i = A_r|H(f_k)|e^{j\phi} * e^{j\theta}$$
$$X_r + jY_r = A_i|H(f_k)|e^{j\phi} * e^{-j\theta}$$

This phase shift can be eliminated by multiplying the both transfer functions, however this leaves the resulting equation with signal dependent noise.

Instead, the phase from both transfer functions will be isolated and multiplied with each other. This eliminates the extra phase shift as well and contributes less signal dependent noise to the theoretical model.

$$(X_i + jY_i) * e^{-j\phi} = A_r|H(f_k)| * e^{j\theta}$$
$$(X_r + jY_r) * e^{-j\phi} = A_i|H(f_k)| * e^{j\theta}$$

The remaining magnitudes can be summed to create a scaled version of the true transfer function magnitude. Combining the phase and magnitude again creates the second proposed theoretical model.

B. *New simulations*

The new model will also be simulated for two different situations. These are the same situations as for the first theoretical model. Simulating this theoretical model returns incredibly inaccurate results. The reason for this is found in the isolated phase. Figure 4 shows the estimated transfer function phase in orange compared to the expected phase in blue for the first situation.

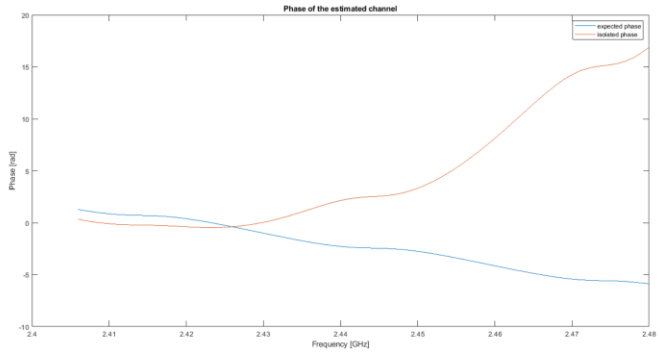

Figure 4: Isolated phase compared to the expected phase for the simulated transfer function of the channel with big difference in path lengths.

The isolated phase increases exponentially while the expected phase decreases linearly.

If the simulation is performed with an estimated phase containing signal dependent noise as in [7], the estimated values for the path lengths match the expected values better. Despite being inaccurate, they vary around the expected values. The estimated magnitude ratio again does not match the expected ratio.

Table 4: Overview of the analyzed situations with signal dependent noise present.

Situation	Type of path	Estimated length r [m]	Estimated magnitude ratio
1	LoS	2.6628	0.8410
	Reflected	13.8461	
2	LoS	1.6936	0.6436
	Reflected	8.1475	

VI. Conclusion

The first theoretical model is not necessarily an incorrect model. The hardware and measurement method did not match the proposed model which made it impossible to test this model with measured data.

The second model does match the hardware, however the proposed method for isolating the transfer function phase needs to be adjusted. The method for finding the transfer function magnitude in this model can be concluded to be correct.

The path length estimations return more accurate results than the path magnitude estimations. Both parameters originate from the same equation. This concludes that the LSE needs to be adjusted to correctly estimate the different path magnitudes. provided some adjustments to the proposed models and methods, it is possible to estimate the multipath channel.

Further research is necessary for the adjustments suggested above. The next step after these adjustments is to integrate a connection with Bluetooth. The system needs to have more than two antennas to allow for practical utilizations. In further research, more complex scenarios can be investigated.

It is hypothesized that the completed proposed theoretical models will work for more than 2 paths as well.

VII. Acknowledgements

I am deeply grateful to all those who provided support for the research presented in this thesis. In particular to my supervisors Prof. dr. Torbjörn Ekman and Prof. dr. ir. Jo Verhaevert for their continuous support, insights and advice regarding this research.

Also, I am grateful to my co-supervisor Carsten Wulff for his advice regarding the hard-ware, as well as Jenny Aune Forbord and Johan Suarez for their support with the hardware setup configuration.

To close, I would like to show my gratitude towards Prof. dr. Herman Van den Broeck and my father Luk Hendrickx for proofreading this thesis.

References

[1] M. Pelka, C. Bollmeyer and H. Hellbrück. ‘Accurate radio distance estimation by phase measurements with multiple frequencies’. In: 2014 International Conference on Indoor Positioning and Indoor Navigation (IPIN). IEEE. 2014, pp. 142–151.

[2] P. Zand et al. ‘A high-accuracy phase-based ranging solution with Bluetooth Low Energy (BLE)’. In: 2019 IEEE wireless communications and networking conference (WCNC). IEEE. 2019, pp. 1–8.

[3] P. Boer et al. ‘Performance of high-accuracy phase-based ranging in multipath environments’. In: 2020 IEEE 91st Vehicular Technology Conference (VTC2020-Spring). IEEE. 2020, pp. 1–5.

[4] P. Zand et al. ‘A high-accuracy concurrent phase-based ranging for large-scale dense BLE network’. In: 2019 IEEE 30th Annual International Symposium on Personal, Indoor and Mobile Radio Communications (PIMRC). 2019, pp. 1–7. DOI: 10.1109/PIMRC.2019.8904093.

[5] S. N. Shoudha et al. ‘Reduced-Complexity Decimeter-Level Bluetooth Ranging in Multipath Environments’. In: IEEE Access 10 (2022), pp. 38335–38350.

[6] United Nations. Sustainable Development Goals. 2023. [Online] URL: https://www.un.org/sustainabledevelopment/ (visited on 9th July 2023).

[7] Core Specification Working Group. Channel sounding. 2023. [Online] URL: https://www.bluetooth.com/specifications/specs/channel-sounding/ (visited on 22nd June 2023).

Contents

List of Figures

List of Tables

Acronyms

BLE Bluetooth Low Energy. 3, 8

CLI Command-line interface. 23, 24

CMD Command Prompt. 23, 24

CT Constant Tone. 8

GDP Gross Domestic Product. 4

IFFT Inverse Fast Fourier Transform. vii, viii, 12, 14, 16, 24–29, 34–36, 38–40

LO Local Oscillator. 8, 9, 31, 32, 41

LoS Line of Sight. 2, 7–9, 12–14, 16–19, 22, 24, 28, 34, 38

LSE Least Squares Estimation. 3, 8, 11, 34, 41

MCPD Multi Carrier Phase Difference. vii, 2, 3, 5, 7–10, 12

MUSIC Multiple Signal Classification. 3, 16

SDGs Sustainable Development Goals. vii, 3, 4, 6

SNR Signal to Noise Ratio. 14, 17, 41

UHF Ultra High Frequency. 1, 3

UN United Nations. 3, 4

1 Introduction

This project falls under the broad field of wireless communications. More specific, it is about communication between two antennas. The goal is to estimate the multipath channel between these two antennas. The multipath is created and influenced by the objects surrounding the antennas. As a consequence, movements of these objects and the antennas change the channel. The changes that occur in the estimated channel contain information about the movements of the different objects. So the estimated multipath channel can be used to monitor the objects in its surroundings.

In this section, a brief overview of all the necessary aspects is given. This is followed by a short section on sustainability. Some practical utilizations are devised, taking into account the aspects discussed in the sustainability section.
Notice that the theory presented in this thesis is only a starting point. So the utilizations devised in this section are very hypothetical.

1.1 A brief overview of all the used aspects

Only two antennas will not be enough to detect the direction in which an object is moving. Let alone multiple objects moving. The general setup for this project is given in figure 1. The antennas are used in combination with one object to create a multipath containing only two paths.

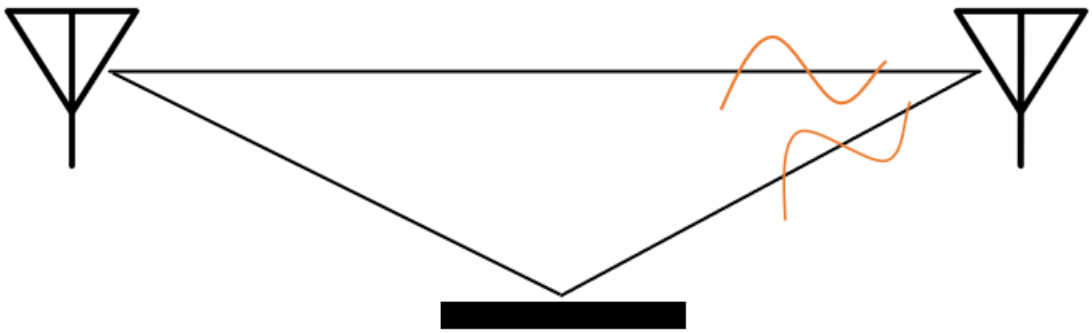

Figure 1: General setup

The antennas are located within $10m$ from each other and are of course communicating with electromagnetic signals. The communication happens in the Ultra High Frequency (UHF) part of the radio frequency bands. This band is often used for communication between devices. Bluetooth also uses the UHF band [1].

If two antennas are communicating with each other, the transmitted signal can take a lot of different paths before it arrives at the second antenna. The combination of all these paths together is called the multipath.

These different possible paths can contain multiple reflections, which causes the signals along these paths to interfere with each other.
If there is a path with no reflections, then the two antennas can see each other. This is called a Line of Sight (LoS).
If measurements are done in an anechoic chamber, only the LoS path is present. This is due to the properties of the anechoic chamber. The anechoic chamber produces reliable results when the transmitted signal is measured since there is no interference of different paths.
To be clear, within the limits of this study, the behavior of a multipath is being examined. This means that a secondary path inside the anechoic chamber needs to be created by the researchers. As a consequence the transfer function of a multipath with exactly two paths can be estimated.

The hardware used in this project for both antennas is Nordic's nRF52833 development kit [2] as shown in figure 2. This development kit has many key features. The most important ones for this thesis are the integrated $2.4GHz$ PCB antenna and the Bluetooth 5.1 multiprotocol radio.
The integrated PCB antenna is specifically designed to be a $2.4GHz$ antenna so it is compatible with Bluetooth. A PCB antenna is also known as a trace antenna. This type of antenna is a metal trace printed on the top layer of the PCB. The advantages of this type of antenna is that it is the most cost effective option. However the antenna is entirely dependent on the ground plane of the PCB. This means that a slight variation in PCB design could cause the center frequency of the antenna to differ from the intended value [3]. The arrow on figure 2 points to the antenna on the board.
The Bluetooth 5.1 multiprotocol radio has a channel selection algorithm integrated. These development kits communicate using Multi Carrier Phase Difference (MCPD). MCPD uses multiple frequency channels while communicating. The channel selection algorithm is necessary for the frequency hopping that accompanies this type of communication with multiple frequency channels.

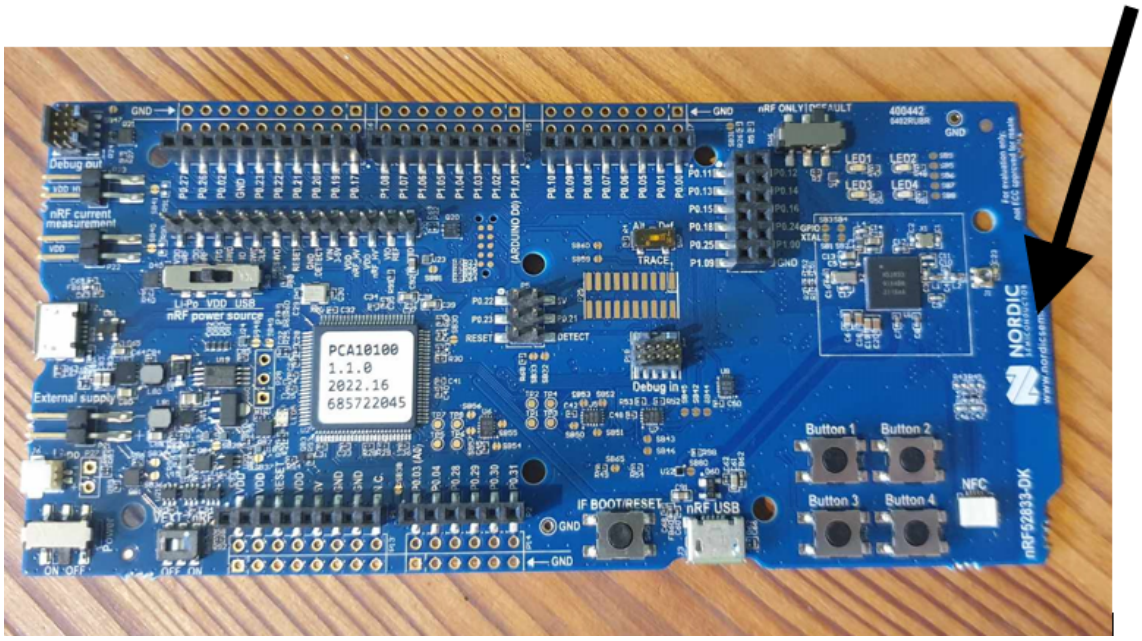

Figure 2: Nordic nRF52833 Development kit

As mentioned above, the development kits use MCPD. This is a ranging method which is often used to measure the distance between two antennas [4].
This is done by first measuring the phase shift between two transmitted frequencies. This phase shift contains information about the distance between the two antennas [5]. MCPD makes use of 40 different frequency bands to get more accurate results. Each different frequency will undergo one phase measurement. The order in which the frequencies will be used, is a unique sequence. This is where the frequency hopping becomes important and thus also the channel selection algorithm accompanying the Bluetooth 5.1 multiprotocol radio. A more detailed explanation about the principle for the distance calculations is given in section 3.1.
When looking at a multipath, the performance can worsen tremendously if it is not taken into account correctly. A lot of research has been done for improving the performance and accuracy of this ranging method in multipath environments. [6] and [7] tell us that the Multiple Signal Classification (MUSIC) algorithm returns the most accurate results even inside a multipath environment.
As explained above, the antennas are operating in the UHF band to be compatible with Bluetooth Low Energy (BLE).

Since the goal is to estimate the multipath channel, only knowing the distance between the two antennas does not provide enough information. In general, the phase shifts introduced by the different paths and the magnitudes associated with the different paths are necessary information to correctly know the channel. To know these values, an estimation is necessary, which leads us to the key theme of this thesis.
In [6], the covariance matrix is used to calculate distances. In a similar way, the covariance matrix in combination with the Least Squares Estimation (LSE) as explained in [8, p. 1041] can be used to estimate the multipath channel.
To realise this estimation, the mathematics enter the domain of matrices. Notice the difference between the hermitian of a matrix and the hermitian matrix itself. The hermitian of matrix M is the same as the conjugate transpose of matrix M, This is noted as M^H. In contrary, if M is a hermitian matrix, then $M = M^H$. This is also explained by [9].

Because the research concerning ranging estimations in multipath environments using MCPD evolves continuously [10], in later stages, this idea can also be expanded to a larger amount of antennas and objects. In this way a whole network can be created that observes all the objects moving inside its multipath channel.

1.2 Sustainability and practical utilizations

In September 2015 , the United Nations (UN) General Assembly adopted 17 Sustainable Development Goals (SDGs) [11], as described in figure 3.
The SDGs consist of clearly defined targets that oversee different domains. Such as social, economic, and environmental challenges. The ultimate goal is to achieve a better future for all people.

Since their adoption, the SDGs have gained significant global importance and have become an important guideline for governments, organizations, businesses, and civil society. Every project or research topic, tries to incorporate sustainable development.

Figure 3: An overview of all SDGs [12]

The SDGs also provide framework for measuring progress and monitoring the outcomes. The UN plays a central role in bringing the idea of the SDGs towards the people. Along with its member states, the UN tracks progress towards achieving the goals and regularly reports on the status of each goal.
Below, while taking into account the SDGs, some practical utilizations are devised for the theory proposed in this thesis. The SDGs that can be linked to the devised utilizations are first given additional explanations. These explanations are each based on the UN's official page on the SDGs [12].

It is important for any organization to evaluate its actions on the basis of the SDGs to contribute to a sustainable future. Can the research proposed in this thesis contribute to one or more of the 17 Sustainable Development Goals (SDGs)?
This study highlights four goals in which opportunities exist to further develop the presented theory into practical applications that can contribute to these development goals.
These four goals are:
Goal 3: Ensure healthy lives and promote well-being for all at all ages
Goal 9: Build resilient infrastructure, promote inclusive and sustainable industrialization and foster innovation
Goal 11: Make cities and human settlements inclusive, safe, resilient and sustainable
Goal 12: Ensure sustainable consumption and production patterns

Today, more than half of the world's population live in cities. By 2050, an estimated 7 out of 10 people will likely live in urban areas. Cities contribute more than 80% of the global Gross Domestic Product (GDP), which makes them drivers of economic growth. This creates more and harder challenges to make cities less polluting, healthier and safer. These challenges inspired goal 11.

A practical application that the theory, presented in this thesis, can contribute to, is the safety of larger cross- roads. With a comprehensive infrastructure, the entire intersection can be monitored. This enables to install even smarter intersection lights, since the system will be able to react quickly to approaching cars and pedestrians it detected.
When for example, something happens to someone while crossing the road, the intersection lights can keep the lights for the cars on red until the person on the crossroad is evacuated.

To achieve goal 9, technological innovation is a really important element. Companies that continuously evaluate and optimize their processes are more resilient to sudden setbacks or extraordinary challenges. High-tech industries perform better and recover faster after a crisis.
A practical example can be found in industry, and more specifically in storage. In warehouses, the goods are often equipped with chips. By integrating antennas and MCPD into these chips, much better warehouse management is possible.
For example, when goods move around the warehouse, their chips communicate with each other. This enables real-time tracking and monitoring of their location, giving warehouse operators accurate and up-to-date information about the location of each item. This minimizes the risk of misplaced or lost goods and acts as an extra security system for unauthorized goods leaving the warehouse as well.

In mid-2022, COVID-19 hit the entire world. The pandemic caused an increase in anxiety and depression, lowered global life expectancy, but also severely disrupted essential health services. Basic treatments could not be carried out in hospitals and rest homes. To this day, the health care sector is even facing severe staff shortages. With these challenges, the progress for goal 3 was halted.
Other than in a warehouse, this system can act as an advanced movement sensor with its ability to map the environment. In this form, the system can also be implemented in nursing homes, which are specially designed to help elderly residents.
The safety of the elderly residents is a top priority in nursing homes. When elderly people fall, there can be serious consequences, especially when they fall inside their room when there are no nurses nearby to provide immediate help. An advanced motion sensor can help alert nurses immediately if something serious happens. This way, staff workload can be reduced while ensuring the safety of all residents.

Unsustainable patterns of consumption and production are root causes of climate change, biodiversity loss and pollution. This threatens human well-being.
Goal 12 implies that governments and citizens must work together to use resources more efficiently. There is also need for reducing the amount of waste and pollution, which will aid in shaping a new circular economy. For this, it is important to use goods efficiently, recycle raw materials and work against overconsumption.
To properly monitor overconsumption and losses, it is important for certain industries to engage in efficient fleet management. This fleet management involves the entire fleet of mobile machinery. By determining the position of the machines on site, it is possible to monitor whether the machines are used efficiently and if they are left unauthorized. If someone tries to steal a machine, this can also be detected.
This way, unnecessary purchases of new machines can be avoided.

This theory is only a small but nevertheless important link in the search for opportunities to create new applications. It is important to think about how a project can contribute to the different Sustainable Development Goals. Focusing on the 17 SDGs automatically creates new opportunities to develop existing or new theories into applications that benefit everyone.

2 Problem description

To the best of my knowledge, most of the research about MCPD right now, focuses on the ranging accuracy in a multipath environment. Channel estimation itself is mostly left alone, with a few exceptions.
Nordic's nRF58233 development kit is already able to estimate the channel between the devices for a LoS environment. However, channel estimation for a multipath environment has not yet been investigated. There is also very little research on practical utilizations with this technique.
Most environments outside an anechoic chamber are multipath environments. Being able to estimate the channel in a multipath environment, will allow more research for practical utilizations. This thesis should act as a starting point for the possible future research topics as well as possible practical utilizations.

In this thesis, the focus lies on the possibility for the multipath channel to be estimated. Therefor, only the situation with two antenna's and one reflecting object will be considered. This results in a multipath with only 2 paths.
The accuracy with which the channel can possibly be estimated is of great importance as well.

3 Theoretical basis

The method used to measure the multipath channel in this paper is based on the MCPD technique. A theoretical model is proposed to represent this multipath channel. To create this theoretical model, a deeper understanding of estimation theory is necessary, more specific about Least Squares Estimation (LSE) In this section, the basic principles behind MCPD will be discussed.

3.1 Multi Carrier Phase Difference

3.1.1 Relation between time, phase and distance

According to [13] The phase shift between two signals $\Delta\phi$ is proportional to the time difference between these signals Δt and the frequency f.

$$\Delta\phi = 2\pi\tau f \tag{1}$$

Consider a setup with two antennas and a LoS between them. The first antenna transmits a signal to the second antenna. This signal arrives with a delay τ_{LoS}. Now the following relation is valid:

$$\tau_{LoS} = \frac{r}{c_0} \tag{2}$$

Where r is the distance between the antennas and c_0 is the speed of light in vacuum. The phase shift that is caused by the channel between the two antennas $\Delta\phi$ can now be written as a function of r. This formula can then be reformed to calculate r when the phase difference in known.

$$\begin{aligned} \Delta\phi &= 2\pi f \frac{r}{c_0} \\ r &= \frac{\Delta\phi\ c_0}{2\pi f} \end{aligned} \tag{3}$$

3.1.2 How is this used in MCPD?

MCPD is a ranging method which uses the above described relation to calculate the distance between two devices. It is compatible with Bluetooth Low Energy (BLE) [4] however, since this thesis only uses 2 antennas, there is no need for a handshake to set up a BLE connection between the 2 antennas. MCPD operates in an $80MHz$ frequency band at $2.4GHz$.

MCPD-ranging introduces two roles, namely the initiator and the reflector. The initiator is the device that starts the measurement and the reflector is the device that responds to the initiator. Figure 4 is based on figure 1 in [4] and represents the communication between the initiator and the reflector. The initiator transmits a Constant Tone (CT) signal with frequency f_k using its Local Oscillator (LO). The reflector receives this signal and performs a phase measurement on it. After some time, the reflector sends back the received signal using its own LO. Now the initiator can perform a phase measurement. Now these

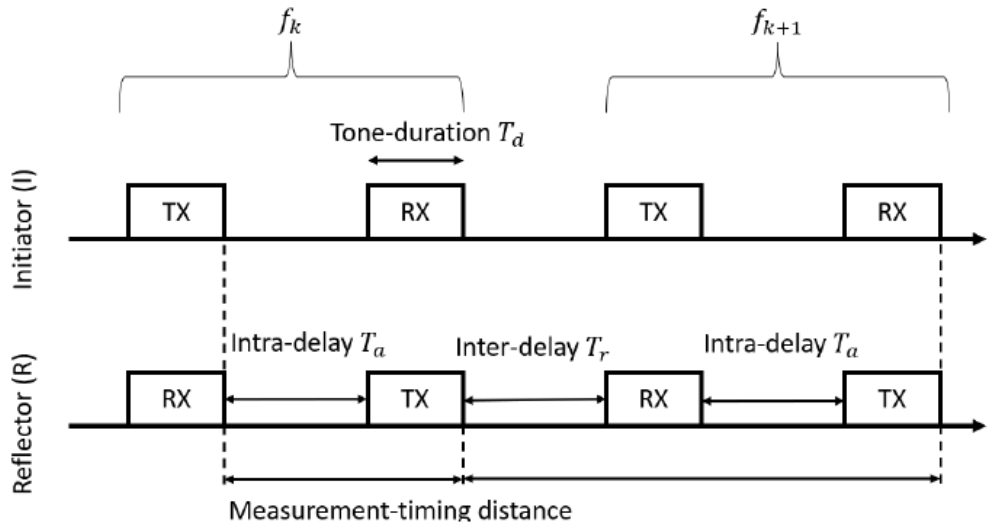

Figure 4: The principle of MCPD ranging

measurements are done for the next frequency f_{k+1}. These measurements are done for all the different frequency channels. However, the sequence is randomly decided and unique. This means that f_{k+1} is not necessarily the frequency channel next to f_k. Because there is only need for synchronization between the clocks of the initiator and the reflector, the phase at the receiving device is only relative to its own LO.

This procedure is repeated for the different carriers in the frequency band. The frequency band is split into 40 channels, each with a bandwidth of $2MHz$.

The phase in a LoS signal can be calculated similar to equation 3.

$$\phi(f_k, r) = -2\pi f_k \frac{r}{c_0} \qquad (mod\, 2\pi) \tag{4}$$

There can be a time offset Δt and a LO-offset θ between the initiator and the reflector. The phase that the reflector will measure is:

$$\phi_R(f_k, r) = -2\pi f_k (\frac{r}{c_0} - \Delta t) - \theta \qquad (mod\, 2\pi) \tag{5}$$

When the roles are switched, the initiator will measure the following phase:

$$\phi_I(f_k, r) = -2\pi f_k (\frac{r}{c_0} + \Delta t) + \theta \qquad (mod\, 2\pi) \tag{6}$$

The measurements taken in the initiator and the reflector are typically both available in the initiator. This means that summing these phases, cancels out the time offset Δt and the LO-offset θ. Notice that the initiator has 80 measurement results, so summing the two results for each specific frequency channel, leaves us with only 40 samples. The signal has now traveled twice the distance, which is clearly demonstrated by equation 7.

$$\begin{aligned} \phi_{2W}(f_k, r) &= \phi_R(f_k, r) + \phi_I(f_k, r) \\ &= -4\pi f_k \frac{r}{c_0} \qquad (mod\, 2\pi) \end{aligned} \tag{7}$$

3.1.3 MCPD multipath

In theory, if the channel consists of multiple paths, the transfer function of the channel can be written as the sum of all these different paths. With each their respective magnitude and phase. For 2 paths this results in equation 8:

$$H(f) = A_{LoS}\, e^{i\phi_{LoS}} + A_{ref}\, e^{i\phi_{ref}} \tag{8}$$

As explained above, the phase of the signal going back and forth is measured. In this theoretical model, the assumption was made that the frequency of the signal sent back by the reflector, is the same as the frequency of the transmitted signal at the initiator. Now the phase shift introduced by the channel is introduced twice. Since the magnitude of $H(f)$ is not a constant over frequency anymore, the magnitude of the transfer function can be written as $|H(f_k|$. Equation 9 shows the transfer function that results after using the MCPD protocol.

Notice the ϵ and the n_n values, which represent the phase noise introduced by the hardware and the noise present in the channel respectively. ϵ_n can be considered constant over frequency for now.

$$G(f_k) = |H(f_k)|\, e^{i(2\phi_k + \epsilon_n)} + n_n \tag{9}$$

In this paper n_n will be neglected. Now the phase in equation 9 is divided by 2 and unwrapped. Again the magnitude of equation 9 is taken to get equation 10. In the next section this equation will be analyzed.

$$\hat{H}(f_k) = |G(f_k)|\, e^{i(\hat{\phi}_k)} \tag{10}$$

3.2 Least squares estimation

Looking at the operating frequencies of MCPD, a carrier frequency of $2.4GHz$ can be defined. Now all the different frequency channels can be split into a frequency carrier and a multiple of the frequency channel width.

$$f_k = f_c + k f_\Delta \tag{11}$$

Where f_Δ is the frequency channel width of $2MHz$ and k is the frequency channel number.
This can be applied to the general equation in 8. Since the transfer function of the theoretical multipath channel is equal to the sum of the individual transfer functions of the different paths, equation 11 can be used to split the general formula into 2 parts as shown in equation 12. The first part of this equation is completely independent of the frequency channel and only differs for the different paths. The second part however is dependent on the frequency channel.

$$\sum_{n=1}^{N} a_n\, e^{(-i2\pi f_c \tau_n)}\, e^{(-i2\pi f_\Delta \tau_n k)} \tag{12}$$

Where n represents the different paths and N the total amount of paths present. Now the following changes can be made. The first part contains information of the magnitude for a specific path n. Let's call this c_n. The second part can be simplified according to the *rootmusic* algorithm used in section 4.2. This gives us the following equations:

$$\begin{aligned} c_n &= a_n\, e^{(-i2\pi f_c \tau_n)} \\ \nu_n &= 2\pi f_\Delta \tau_n \end{aligned} \tag{13}$$

Equation 12 can be changed accordingly. This results in:

$$\hat{H} = \sum_{n=1}^{N} c_n\, e^{-i\nu_n k} \tag{14}$$

Now consider the scenario in which there are only two paths. Based on [6], the equation in 14 can be reformed to make use of matrices. Consider $\hat{H}$ to be a $40\,X\,1$ matrix with the estimated transfer function values for each frequency channel. Let C be a $2\,X\,1$ matrix with the c_k values for the different paths. The matrix A needs to contain the complex part of equation 14 with the ν_n values and the frequency channel numbers k. This results in a matrix with dimensions $40\,X\,2$.

$$A = \begin{bmatrix} e^{-i\nu_1} & e^{-i\nu_2} \\ e^{-i\nu_1 2} & e^{-i\nu_2 2} \\ \dots & \dots \\ e^{-i\nu_1 40} & e^{-i\nu_2 40} \end{bmatrix} \tag{15}$$

Using the LSE [8, p. 1041], the values for C can be calculated by using A^H. This is the conjugate transpose of matrix A.

$$\begin{aligned} \hat{H} &= A * C \\ C &= (A^H\, A)^{-1} A^H\, \hat{H} \end{aligned} \tag{16}$$

Now first of all, the values for τ_n can be calculated using ν_n. This means that the time delay for each path is known. Since equation 16 allows us to calculate the values for c_n, all the information necessary to calculate the magnitude a_n is present.
The time delay and the magnitude for each path in the multipath are sufficient information to completely describe the transfer function of that multipath.

$$\begin{aligned} \tau_n &= \frac{\nu_n}{2\pi f_\Delta} \\ a_n &= \frac{c_n}{e^{(-i2\pi f_c \tau_n)}} \end{aligned} \tag{17}$$

4 Simulations

To simulate the channel, Matlab was used. First a channel containing only one LoS-path was simulated. This way, a deeper understanding was obtained on the properties of a channel. Following this, the multipath channel was created and simulated. As previously mentioned in section 2, this channel contains one LoS-path and one reflected path.

4.1 One path: Line of Sight

The virtual environment that was created to simulate this model, consists of 2 antennas with a distance of $5m$ between them. Complex Gaussian noise with a variance of 0.001 was added to the channel to better resemble the real world. Because MCPD was used, the phase can be expressed with equation 7. The Fourier transform of a channel can be set up using only phase and magnitude. Since there is only one path, the magnitude is neglected to simplify the equation.

$$H(f_k) = e^{-i\,4\pi f_k \frac{r}{c_0}} + Noise \tag{18}$$

To find the behaviour of the channel in the time domain, the Inverse Fast Fourier Transform (IFFT) of equation 18 was taken. The x-axis was scaled to represent time delays. The result is shown in figure 5. Notice that the peak corresponds to the time delay present in the created channel. This delay values $16.7188\ ns$. Using equation 2, the distance between the antennas can be calculated:

$$\begin{aligned} r = \tau_{LoS}\ c_0 &= 16.7188 * 10^{-9}\ s * 3 * 10^8\ m/s \\ &= 5.0156m \end{aligned}$$

This calculated distance only differs $1.56cm$ from the real value. This This translates to a relative error of 0.312%, which means that the implemented model can be considered accurate.

4.2 Multipath: LoS + one reflection

For the multipath simulations, three scenarios will be simulated. In the first scenario, there is a big difference in length between the paths. In this scenario the LoS-path will be $5m$ and the reflected path will be $15m$. Creating a difference in path length of $10m$. The second scenario has a much smaller difference between their path lengths to represent a more realistic situation. Since measurements will be done in an anechoic chamber, the possibilities for these paths become very restricted. Because an anechoic chamber is not that big, the path length difference will be a lot smaller compared to the first simulation. A difference of $1m$ was established using a LoS-path of $5.1m$ and a reflected path of $6.1m$. Since there are now two paths present, the IFFT will contain two peaks. Finding these two peaks can be significantly harder and less accurate than finding only one peak. Luckily Matlab has a function called *rootmusic*, which can easily find these two peaks.
Before the simulations can be done, the maximum possible amplitude for the signal traveling along the reflected path needs to be examined.

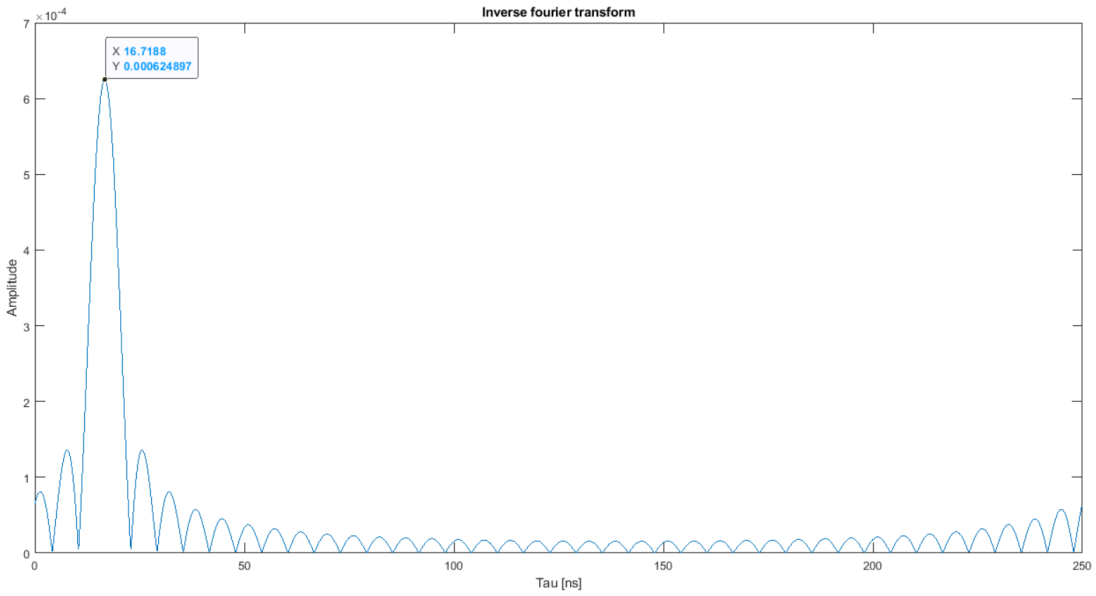

Figure 5: One path LoS channel behaviour in time domain

4.2.1 Relation between magnitude and path length

In the multipath simulations, the magnitudes of the different paths cannot be neglected anymore. However, they can be normalized. Consider the magnitude of the LoS path to be one. Then the magnitude of the reflected path is always less than 1. Because the longer a signal travels, the more it is attenuated.
To calculate the received power for the reflected path, the following equation can be used [14]:

$$P_R = P_0 \left(\frac{d_0}{d} \right)^{\gamma} \tag{19}$$

Where d_0 is a reference distance and P_0 the received power at this distance. d is the distance between the antennas for which the received power needs to be calculated and γ is the path loss exponent.
Notice that the values d_0 and P_0 are the same for the LoS path and the reflected path. Since the received power is proportional to the magnitude squared, the following relation is valid.

$$\begin{aligned} \frac{A_{ref}^2}{A_{LoS}^2} &= \frac{P_0(\frac{d_0}{d_{ref}})^{\gamma}}{P_0(\frac{d_0}{d_{LoS}})^{\gamma}} \\ \left(\frac{A_{ref}}{A_{LoS}} \right)^2 &= \left(\frac{d_{LoS}}{d_{ref}} \right)^{\gamma} \end{aligned} \tag{20}$$

The path loss exponent γ is a value between two and five. Notice the reflected path is always longer than the LoS path. This means that the right part of equation 20 decreases with an increasing γ. The lowest possible value for γ is two, this results in the following inequality.

$$\left(\frac{A_{ref}}{A_{LoS}}\right)^2 \geq \left(\frac{d_{LoS}}{d_{ref}}\right)^2$$

$$\begin{aligned} d_{ref} &\geq \left(\frac{A_{LoS}}{A_{ref}}\right) d_{LoS} \\ A_{ref} &\leq \left(\frac{d_{LoS}}{d_{ref}}\right) A_{LoS} \end{aligned} \tag{21}$$

4.2.2 Big difference in path length

This scenario has a LoS path length of $5m$ and a reflected path length of $15m$. Taking into account equation 21, the reflected path magnitude A_{ref} can be no greater than $1/3$ of the LoS path magnitude A_{LoS}. Since the LoS path is considered to be 1, let A_{ref} be 0.3

Together with the amplitudes, the noise present in the setup needs to be integrated as well. Equation 9 explains which types of noise are present in the transfer function of the channel. For n_n a complex Gaussian distribution with a variance of 0.001 was chosen. This means that the channel has a really good Signal to Noise Ratio (SNR) of $60dB$. The hardware noise ϵ_n can be considered the same for all the different frequencies f_k for now. Figure 6 shows the IFFT of the channel's transfer function. Notice that there are now two peaks located at $16.6736ns$ and $50.0047ns$ respectively. Again the corresponding distances can be calculated, which are $5.0021m$ and $15.0014m$ respectively.
The error on the true distance is only a few millimeters. The relative error for the LoS path and the reflected path is 0.042% and 0.0093% respectively.
With small noise levels, the length estimation is really accurate, however in the real world, there is typically a lot more noise. Table 1 shows the influence of different values for the SNR. As suspected, when there is more noise present, the estimations become less accurate. Notice that the reflected path length estimations are more susceptible to noise than the LoS path length estimations.

Table 1: The influence of SNR on path length estimations for a big path length difference

SNR	LoS path [m]	Relative error [%]	Reflected path [m]	Relative error [%]
$60dB$	5.0021	0.042	15.0014	0.0093
$40dB$	4.9742	0.516	15.0920	0.613
$20dB$	4.9589	0.822	16.1694	7.796

Figure 7 shows the estimations for the magnitudes accompanying each path in orange. In blue, the initial values are shown. The estimated values are much lower than the initial values. This can be considered a scaling error, which can be ignored by normalizing the reflected paths to the LoS-paths. For the initial values this gives a ratio of 0.3. However for the estimated values, this ratio is around $3/5$.
This ratio does not change when the initial values for the magnitude are different. Instead only changes occur when the path lengths for the LoS path and the reflected path change.

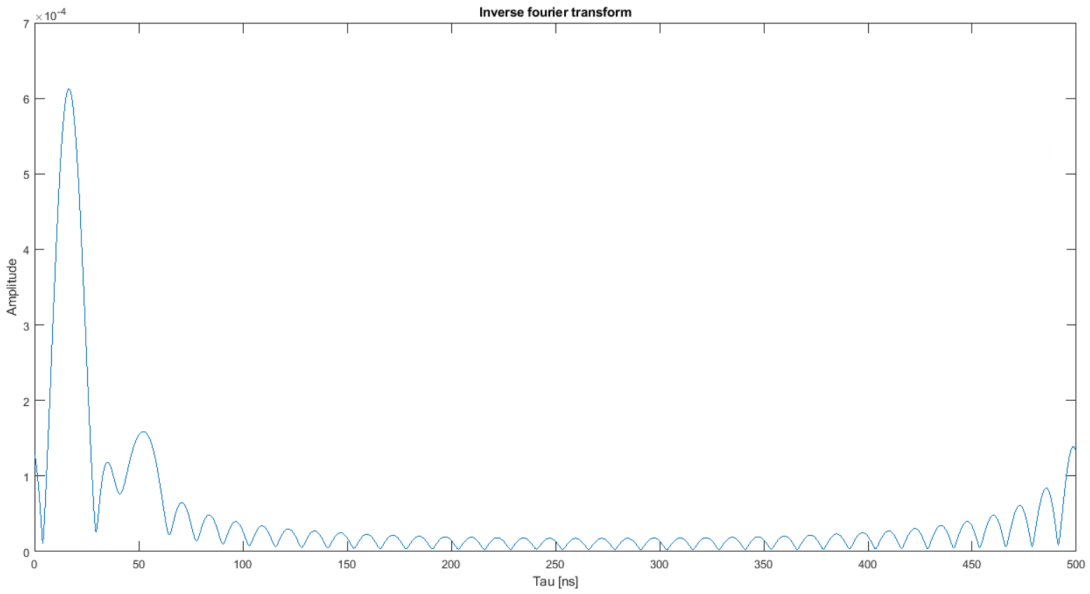

Figure 6: Multipath channel behaviour in time domain for path lengths $5m$ and $15m$

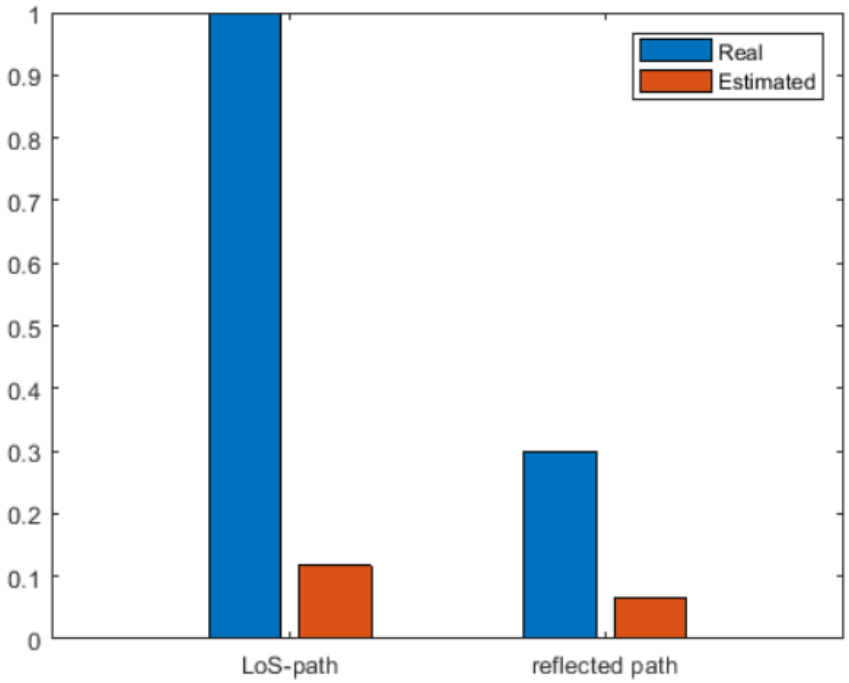

Figure 7: Estimated magnitudes compared with the real magnitudes for a big difference in path length

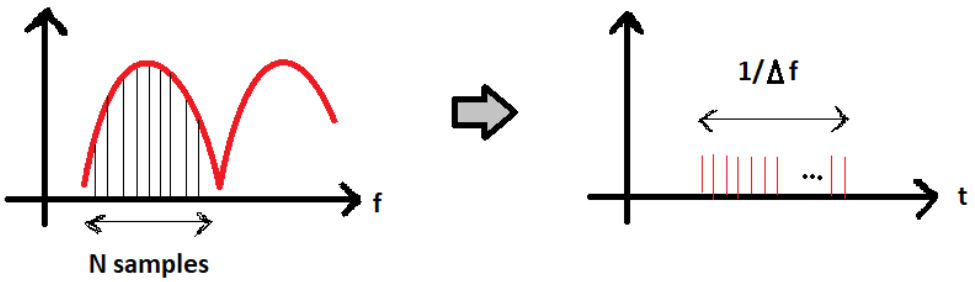

Figure 8: The effects of quantizing and windowing for the time- and frequency domain

4.2.3 Small difference in path length

As explained above, the LoS-path length is $5.1m$ and the reflected path length is $6.1m$. This creates a difference of $1m$. Figure 9 shows the IFFT of the channel transfer function. Notice that there is only one peak in contrary with the previous simulation.

This has to do with the resolution bandwith [15] [16]. Since the measurements are taken for different frequency channels in the frequency domain, the transfer function of the channel is quantized. Since there are 40 frequency channels used, the number of samples N is 40 as well. The distance between these frequency channels is called the frequency step. If the transfer function in the frequency domain is sampled and thus quantized, the IFFT of the transfer function in the time domain will have a limited range. This is called a window. The opposite is true as well. So if the transfer function in the frequency domain is limited in range, the IFFT in the time domain will be discrete. Figure 8 shows this relation.
The window size in the time domain is now $1/\Delta f$. Since there are 40 channels, the resolution in the time domain becomes better, resulting in 40 different areas inside this window. The width of these areas is also called the resolution.
Whenever the distance between two peaks is less than the resolution, only one peak will show up. Below the resolution in the time domain and the corresponding distance are calculated.

$$\begin{aligned} Resolution_t &= \frac{1}{N\Delta f} \\ &= \frac{1}{40 * 2MHz} = 12,5ns \end{aligned} \tag{22}$$

$$\begin{aligned} Resolution_r &= \tau * c_0 \\ &= 12.5ns * 3 * 10^8 m/s = 3.75m \end{aligned}$$

Since the path length difference is smaller than the resolution, only one peak is visible in the transfer function.
When this happens, the MUSIC algorithm in matlab can still find the time delay values τ for the two paths.

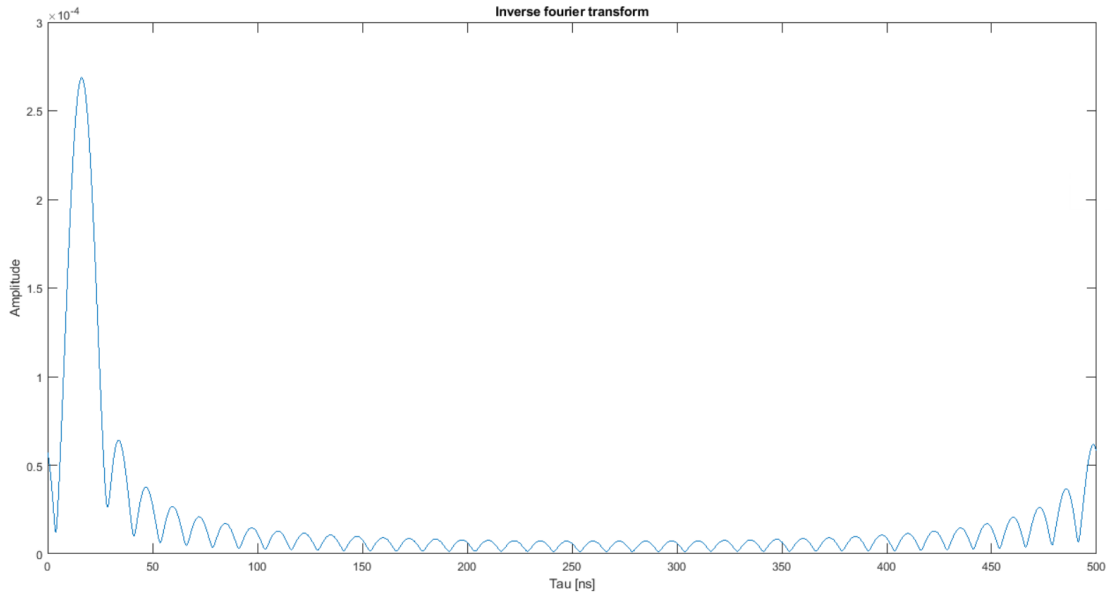

Figure 9: Multipath channel behaviour in time domain for path lengths $5.1m$ and $6.1m$

For the LoS-path and the reflected path respectively, τ is $16.9255ns$ and $20.2208ns$. This results in path lengths of $5.0777m$ and $6.0662m$ respectively. The relative errors compared to the expected values are 0.446% and 0.563% respectively.
Table 2 was constructed to analyze the influence the SNR has on these estimations. The error for $60dB$ SNR is already greater than for the big difference in path length. Since a smaller difference means that the paths are more difficult to distinguish from each other, this is to be expected. Similar to the previous case, the reflected path length estimation is more susceptible to noise than the LoS path. For a $40dB$ SNR, the relative error is already 40.2%. For a $20dB$ SNR, the noise completely includes the reflected path.

Table 2: The influence of SNR on path length estimations for a small path length difference

SNR	LoS path [m]	Relative error [%]	Reflected path [m]	Relative error [%]
$60dB$	5.0777	0.446	6.0662	0.563
$40dB$	5.2364	2.67	8.5534	40.2
$20dB$	5.2675	2.75	/	/

Figure 10 shows the estimated magnitudes for the different paths. Again there is a normalization problem which can easily be taken care off as explained above. The ratio of the estimated magnitudes for the two paths, is around $4/5$. This is again not the expected ratio of 0.3.

The next step is to compare the estimated values for the big difference in path length with the estimated values for the small difference in path length. Since no additional rescaling was applied between running the two simulations, it can be noticed that the small difference in path lengths gives higher estimated values for the magnitude. This is due to the smaller reflected path length. A longer path will contribute more attenuation, resulting in a smaller magnitude.

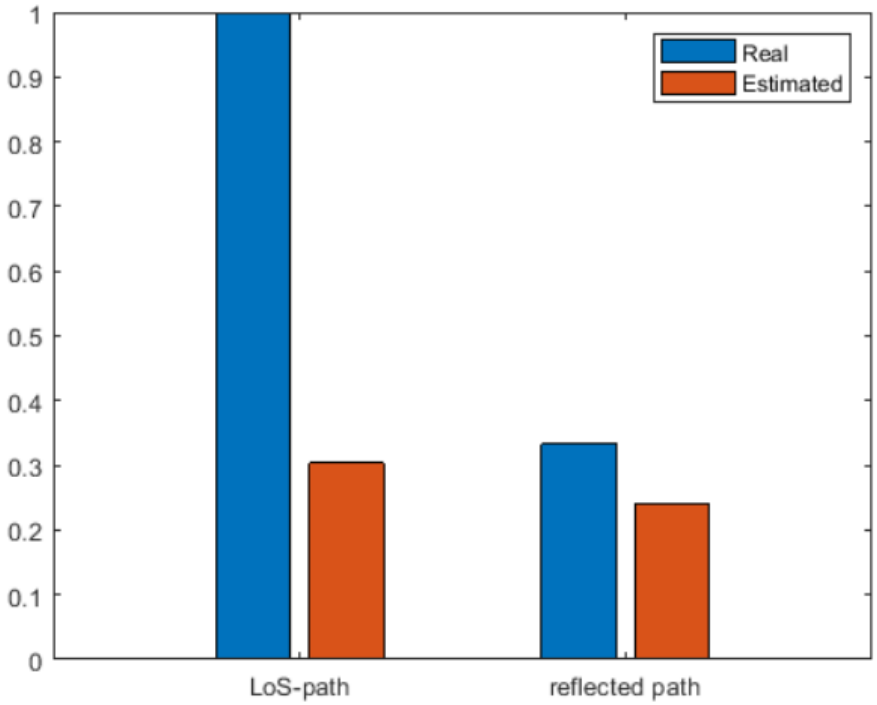

Figure 10: Estimated magnitudes compared with the real magnitudes for a small difference in path length

From this data it can be concluded that the LoS magnitude simulation is influenced by the reflected path in some way, Since the ratio of the magnitudes is mostly influenced by the different path lengths. The magnitude corresponding to the reflected path is slightly smaller than the magnitude of the LoS path. From this follows that the ratio of the reflected path magnitude to the LoS path magnitude is much greater than 0.3.

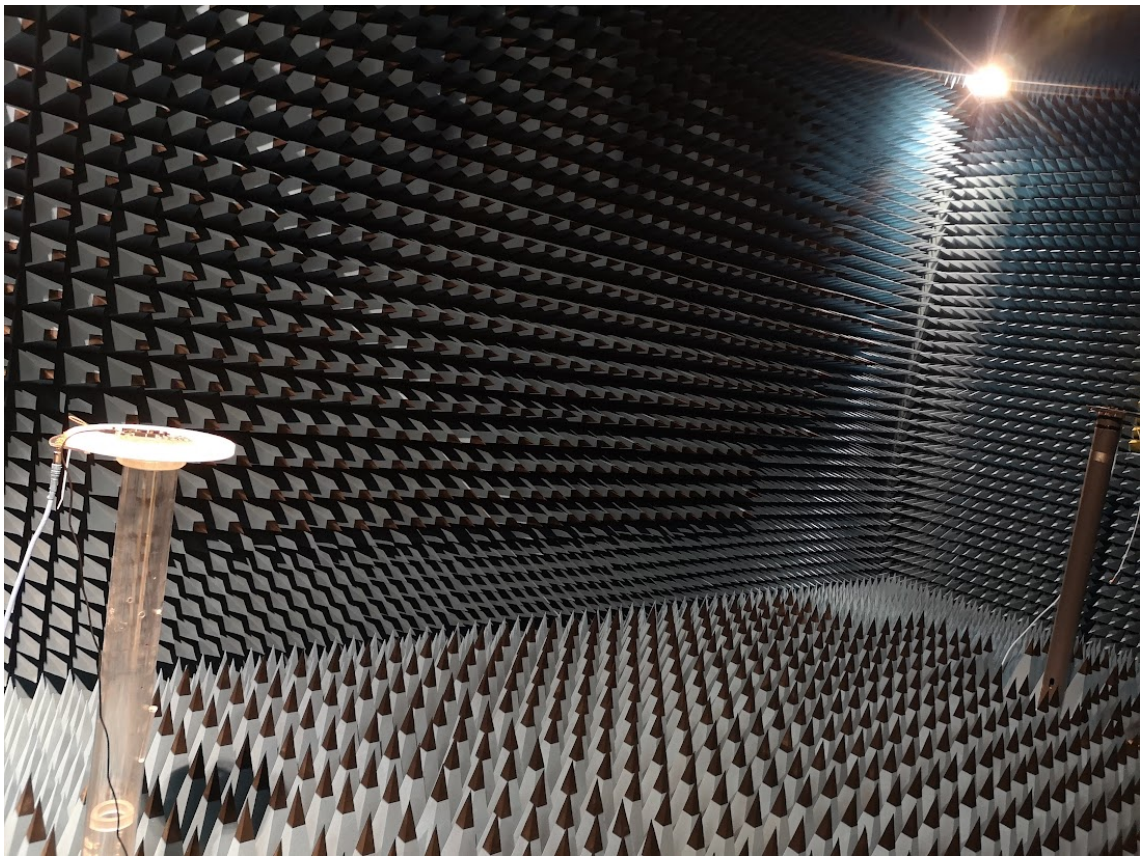

Figure 11: Initiator antenna (left) and reflector antenna (right) in the setup in an anechoic chamber

5 Measurements

Simulating a theoretical model is not enough to validate the model. Simulations give a general picture about the behavior of the model. But to really validate a theoretical model, measurements in real life are necessary as well.
As mentioned above, the theoretical model proposed in this paper will be tested using measurements made in an anechoic chamber. The anechoic chamber places some restrictions on the possible lengths for the two paths. First, the places for both initiator and reflector antenna are fixed locations in the room. These can be seen on figure 11. Furthermore, the anechoic chamber is limited in size. The locations where the reflecting object can be placed inside the room are limited in number as well.
The channel was measured for three different scenarios.

5.1 Setup

The initiator and the reflector are both placed on their fixed holders. The distance between these two locations is measured with a laser rangefinder. This distance will be the same for all three scenarios and values $5.1m$. The LoS path length is thus $5.1m$.
For the reflected path length, there is a little more freedom. Figure 12 and figure 13 show the reflecting object in the anechoic chamber from the point of view of the reflector and

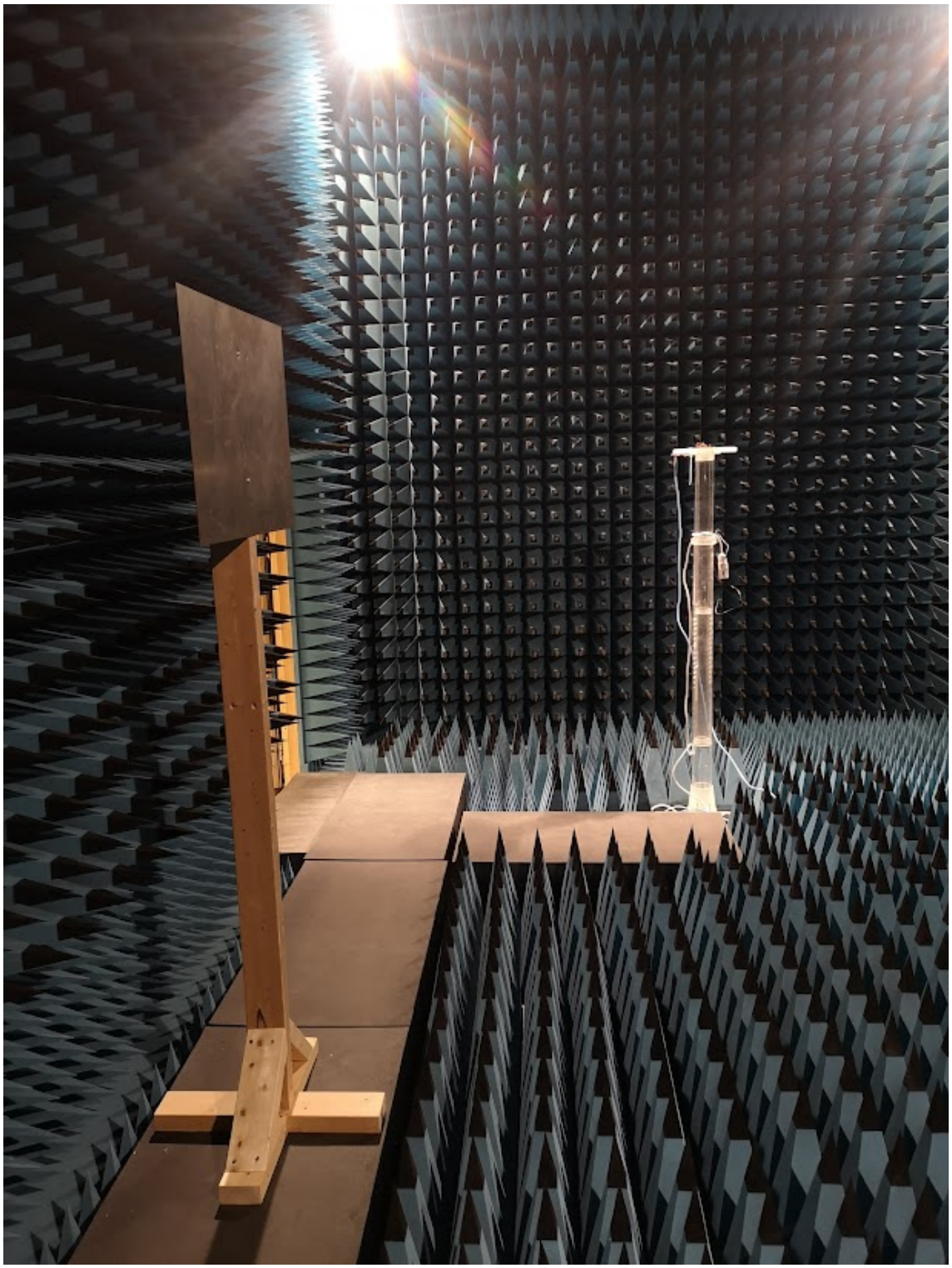

Figure 12: reflecting object from the point of view of the reflector antenna

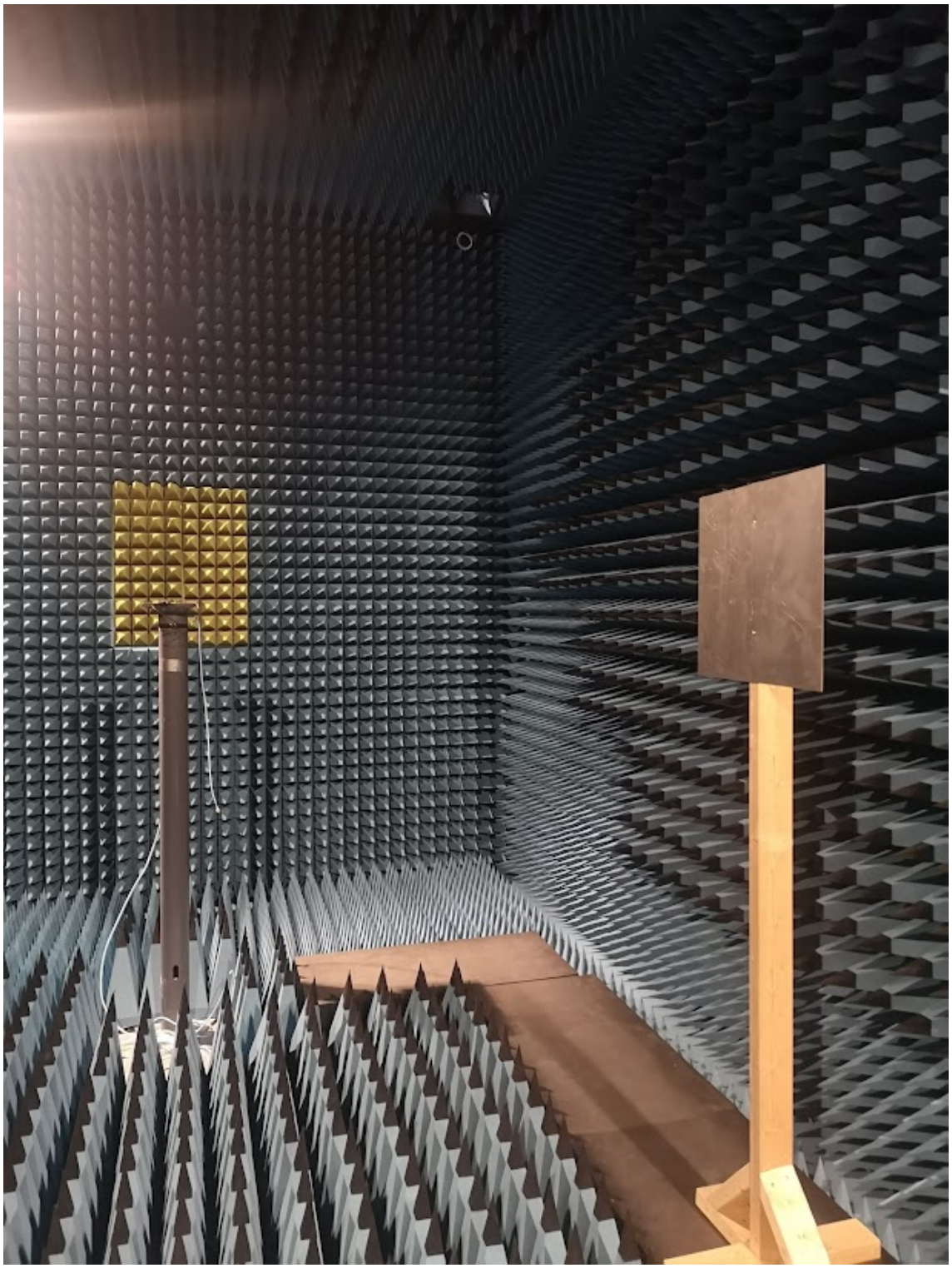

Figure 13: reflecting object from the point of view of the initiator antenna

the initiator respectively. Notice the small black path which allows the researchers to walk from the first antenna to the second. The reflecting object can only be located somewhere on that path.
On the reflecting object, a small dot was drawn to make it easier to aim while using the laser rangefinder. The reflected path lengths are thus first measured with a laser rangefinder as well. This allows for good references.

In the first scenario, the reflecting object is placed in the middle between the antennas. This ensures that the reflected path has it's shortest possible length. Figure 14 shows an eagle view of this scenario with the reflecting object visualized in red. The reflected path length here is $6.1m$ long, resulting in a path difference of $1m$.
The realistic simulations are based on this scenario and the results from this scenario will thus be compared to the simulations in section 5.2.

In the second scenario, the object has moved towards the reflector antenna. This can be seen on figure 15. The object is located $1/4$ of the LoS path length away from the reflector and $3/4$ away from the initiator. The reflected path in this scenario has a length of $6.3m$.
Notice that the reflecting object is slightly tilted. This is to ensure that the signals reflecting from the object, will definitely reach the antennas.

The third scenario has the longest possible length for the reflected path. This is accomplished by placing the reflecting object on a line with the reflector antenna and as far in the corner as possible. This is shown in figure 16. Using the laser rangefinder, the length of this path is $6.6m$.

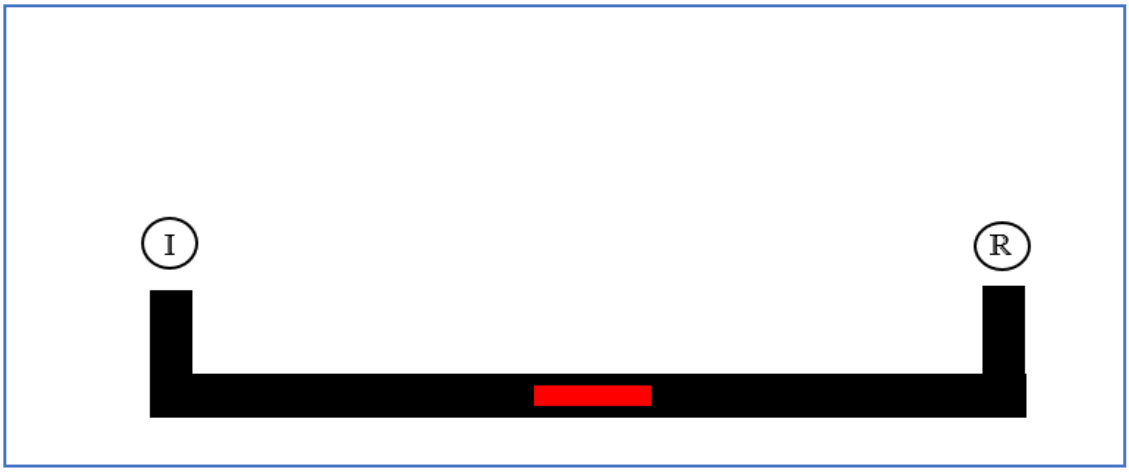

Figure 14: Lab layout of the first scenario

Figure 15: Lab layout of the second scenario

Figure 16: Lab layout of the third scenario

5.2 Analyzing the results

5.2.1 From hardware to computer

Before the measurements can be analyzed, it must be understood how the data moves from the hardware to the computer.
A general image of the communication between hardware and computer is given in figure 17.
On the computer, the Command Prompt (CMD) is running. This allows for faster interactions. To realise this, the 'nRF connect for desktop' software needs to be installed [17]. The make-file in the git repository in [18] can be used to initialize the hardware from the command line. The initiator and reflector are initialized by first connecting them to the computer and then running the command *make flashi* and *make flashr* respectively. Since the measurements are available at the initiator antenna, this antenna needs to stay connected to the computer.
The git repository is also equipped with python code to control the hardware. A Command-line interface (CLI) ensures that specific functions from this python code can be called

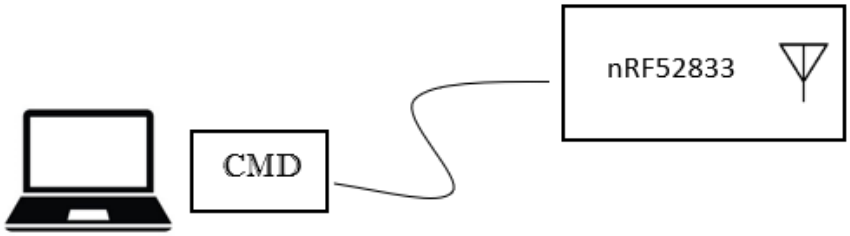

Figure 17: How the nRF52833 is connected to the computer

upon from the Command Prompt. Now the computer acts as a medium for the researchers to first initiate the measurements and then access the results.
In the Command Prompt (CMD), using the python CLI, the measurements can be initialized with the functions *save* and *msave*. The function *save* makes only one measurement while *msave* makes multiple. The number of measurements is determined by the variable count. The argument COM, needs to be the serial port number where the initiator is connected to. The measured data is stored inside a JSON file or a directory with JSON files respectively. This file or directory is new and thus created by the python code itself. These JSON files contain I and Q values, with which the transfer function of the channel can be reconstructed as shown in equation 23.

$$I + jQ = A|H(f_k)|e^{j\phi} \tag{23}$$

The python code contains different functions as well to analyze the results, which will not be used in this thesis. Instead, a second python script named *to_matlab* was written. This piece of code is also equipped with a CLI. It will take all the JSON files from a given directory, reconstruct the average transfer function and return this in a .txt file. This .txt file can be analyzed in matlab.

5.2.2 Measurement results

After analyzing the measurement results, again the IFFT of the channel transfer function is obtained as well as the magnitudes associated with the two paths.
Figures 18 and 19 show the results for the first scenario with path lengths $5.1m$ and $6.1m$. In figures 20 and 21, the results for the second scenario with path lengths $5.1m$ and $6.3m$ are visualized.
The results for the third scenario, with path lengths $5.1m$ and $6.6m$, are shown by figures 22 and 23.
Using the *rootmusic* algorithm as explained in section 4.2, the values for τ corresponding to the two paths, can be found. Using equation 2, the path lengths can be calculated. Table 3 contains the lengths and magnitudes corresponding to the paths for the different scenarios.

First the magnitudes of the two paths for the different scenarios are analyzed. Again the ratio of reflected path magnitude to LoS path magnitude does not have the expected value. Instead the ratio is 0.8651 for the first scenario, 0.9565 for the second scenario and 0.9262 for the third scenario.

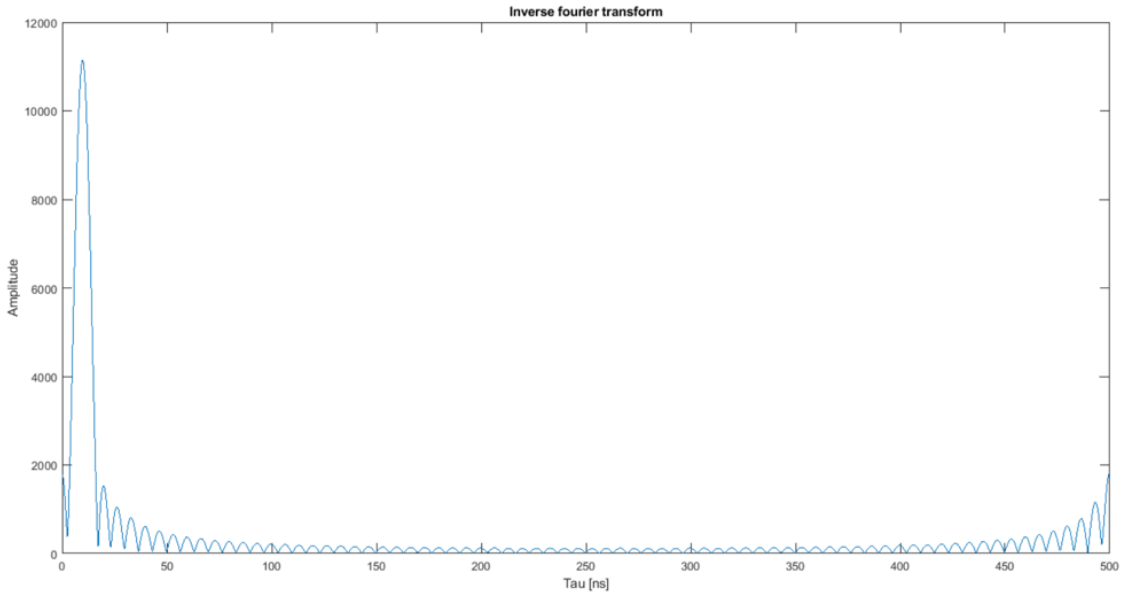

Figure 18: IFFT of the channel transfer function with path lengths $5.1m$ and $6.1m$

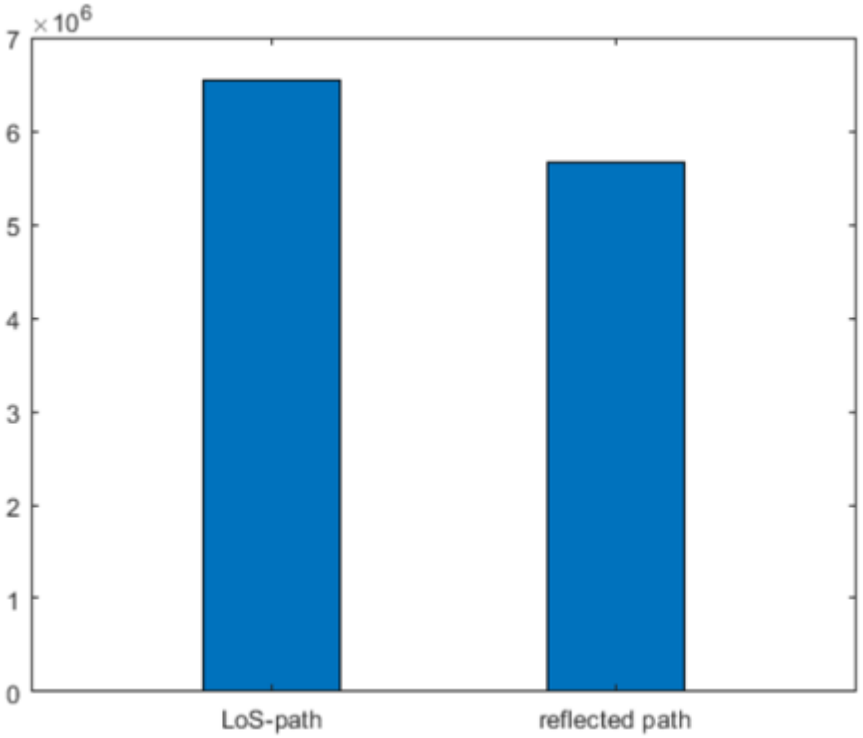

Figure 19: Magnitudes of the paths for path lengths $5.1m$ and $6.1m$

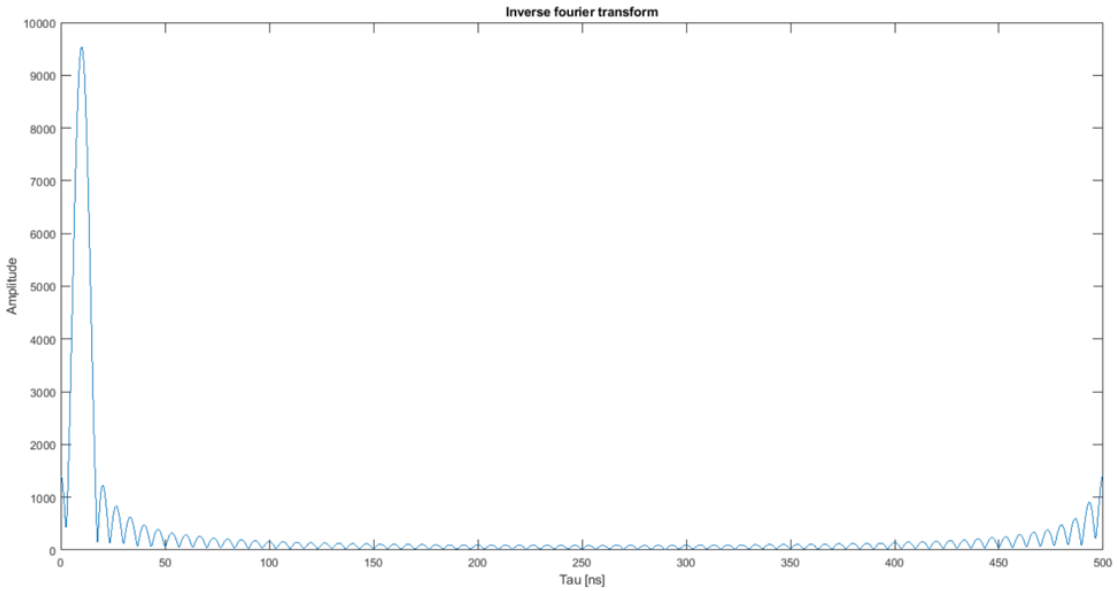

Figure 20: IFFT of the channel transfer function with path lengths $5.1m$ and $6.3m$

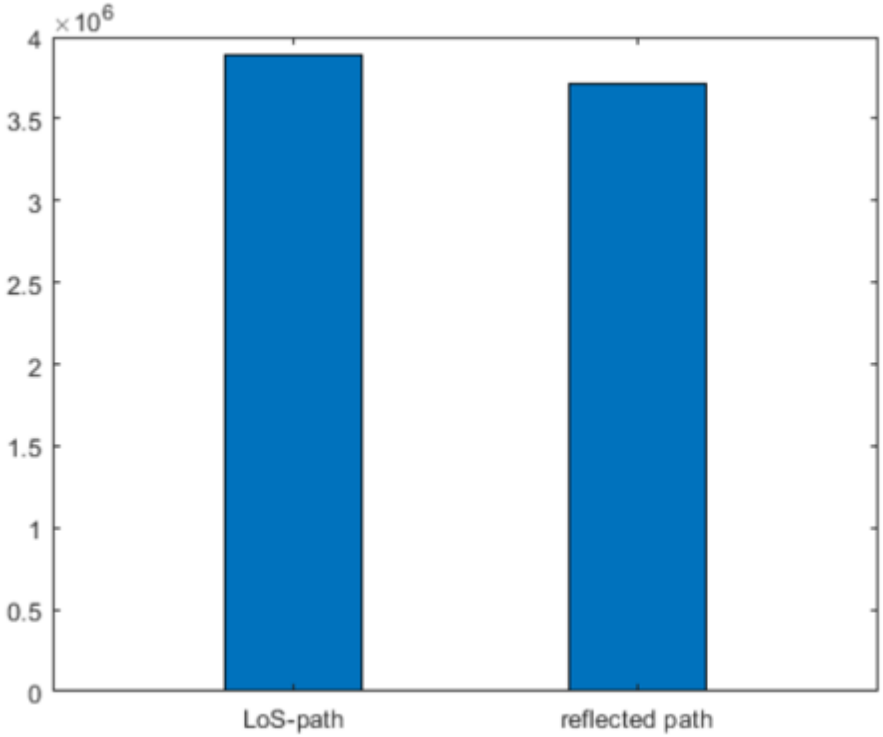

Figure 21: Magnitudes of the paths for path lengths $5.1m$ and $6.3m$

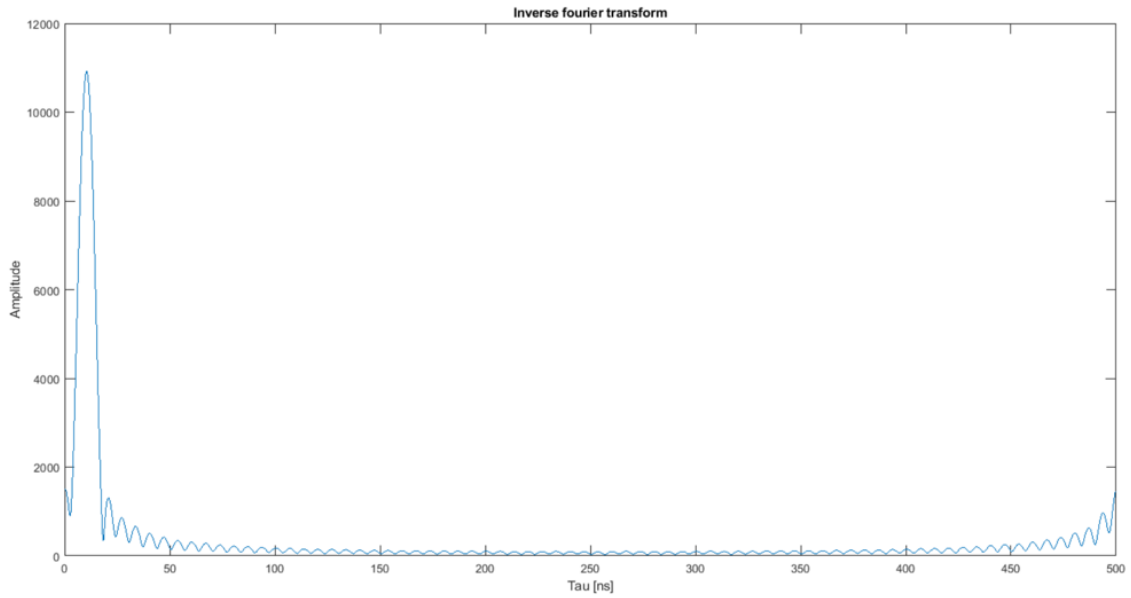

Figure 22: IFFT of the channel transfer function with path lengths $5.1m$ and $6.6m$

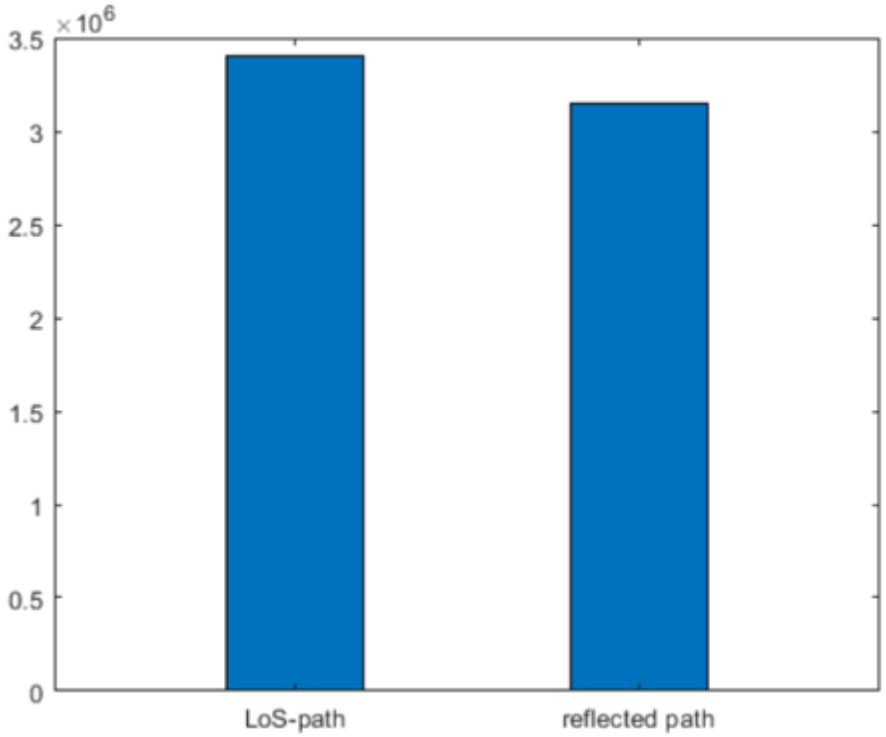

Figure 23: Magnitudes of the paths for path lengths $5.1m$ and $6.6m$

Table 3: Results after analyzing the measured transfer functions

Real length of reflected path [m]	Type of path	Estimated length [m]	Magnitude ratio
6.1	LoS	2.5246	0.8651
	Reflected	3.4444	
6.3	LoS	2.5712	0.9565
	Reflected	3.6874	
6.6	LoS	2.6233	0.9262
	Reflected	3.8380	

It is noticeable that in all 3 scenarios, the reflected path magnitude is slightly smaller than the LoS path magnitude. This observation is consistent with the conclusions that can be drawn from the simulations

Looking at the estimated path lengths, they too are not similar to the expected values. Instead they look to be more in line with half the expected values. Table 4 compares the different path lengths with their doubled value and indeed they are more similar to the expected results according to the theoretical model and the simulations. However, the reflected path lengths doubled are still slightly off by about $1m$.

Table 4: Measured values for the path lengths in the different scenarios

Real length of reflected path [m]	Type of path	Estimated length [m]	Doubled[m]
6.1	LoS	2.5246	5.0492
	Reflected	3.4444	6.8888
6.3	LoS	2.5712	5.1424
	Reflected	3.6874	7.3748
6.6	LoS	2.6233	5.2466
	Reflected	3.8380	7.6760

5.2.3 Comparison to simulations

Figure 24 shows the IFFT of the channel transfer function. The measured and simulated IFFT's are shown in blue and orange respectively.
Notice that the peak in the blue curve is located on a smaller τ than the peak in the orange curve. This is again explained by the fact that the measured lengths value only about half the expected lengths.
Both curves were normalized, to allow for a better comparison.

The magnitudes for the measured and estimated paths, are visualized in figure 25. Notice that the magnitudes are both normalized so that the LoS path magnitude equals one.
The same conclusion can be drawn as before. That is, the magnitudes for the reflected path are slightly smaller than the magnitudes for the LoS path. The ratio for the measured and the simulated values are in the same range. However, since there is only one data set for the scenario with a reflected path length of $6.1m$, the influence of noise on the magnitude estimation can not be taken into account.

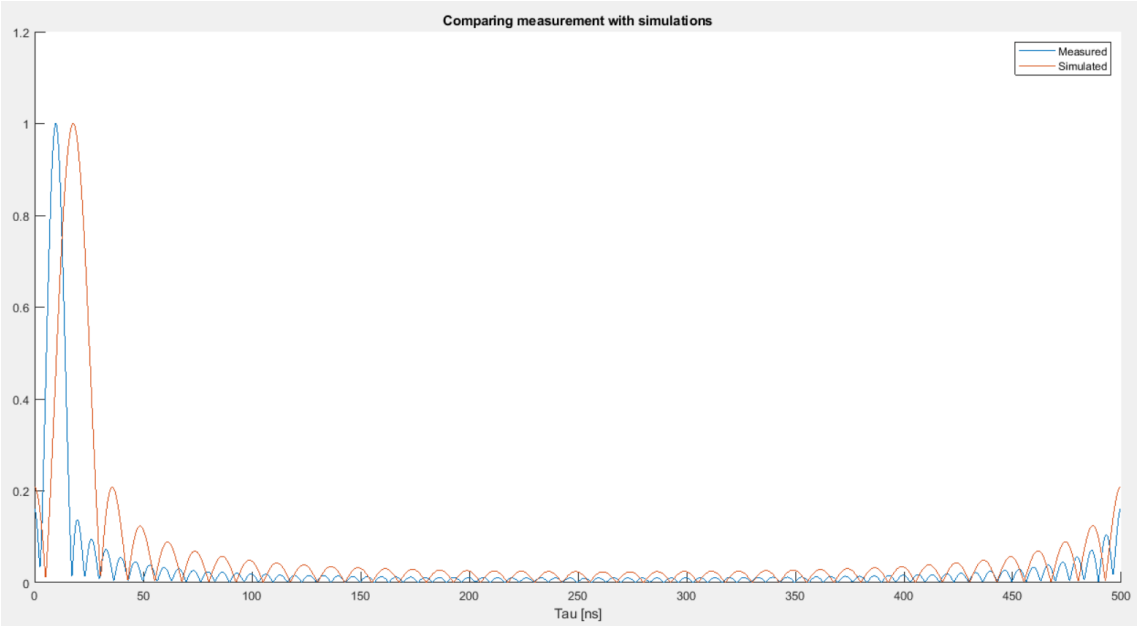

Figure 24: Comparison of the normalized IFFT for the simulated- and the measured transfer function

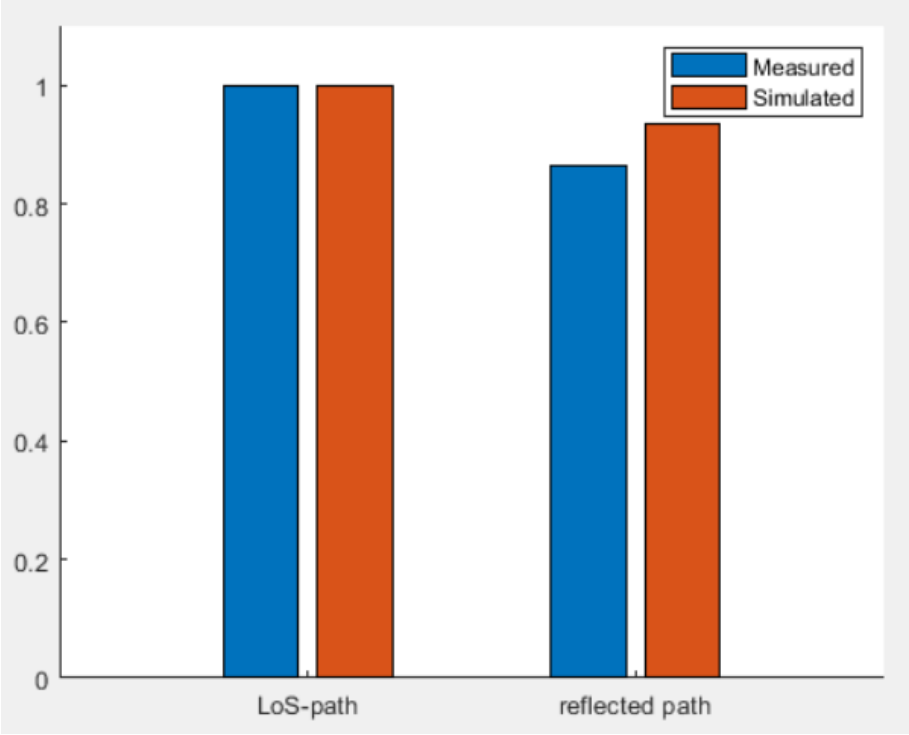

Figure 25: Comparison of the normalized magnitudes for both paths

This means that despite looking similar, no conclusions can be drawn about the consistency with which the ratios are truly similar.

5.3 Conclusion

The measurements as well as the simulations do not match the theoretical model.
It is noticeable that, where the simulations give the expected results for the path length estimations, the measurements still don't match the presented theoretical model.
As explained in section 5.2, the path lengths measured using the hardware are in the range of half the expected lengths. This points towards an incorrect assumption made about the hardware. A deeper look inside the nRF52833 development kit is necessary to try and figure out what exactly happens when measuring a transfer function. The following questions that need to be answered are, if and how this differs from the presented theoretical model.
The theoretical model will have to be revised as well. If the hardware measures the transfer function slightly different than expected, the possibility exist that the measurements are influenced by an extra factor. The existence of an extra noise factor which was not taken into account, is also a possible effect that can occur when the hardware does not match the theoretical model.
Since the hardware is fixed and will always measure the transfer function of the channel in the same way, the theoretical model will have to be changed accordingly.

{"i_local": [0, 0, 0, 0, 2592, 576, -2720, -5600, 9216, 8128, -5792, -2976, -9984, 10304, 7680, -10208,
64, -4000, 2560, 5312, 7040, -9568, 3328, -9344, -7840, -9152, -9600, -7808, -2240, 6080, -9664, 8480,
8000, -9696, -9504, -9632, 7008, 1856, -7040, 8640, 8512, -8480, 9120, -3008, 8192, -4256,
1408, -8224, -4032, -3360, -7360, 7616, 4960, 8320, -32, 7616, -8320, -8064, -5792, 5472,
8160, -6016, -8096, -2400, 1184, -7904, 4064, -7808, -5600, 7264, -7712, -7776, 2016, 6880, 6880, 7392, 896,
7136, 1216, 0], "q_local": [0, 0, 0, 0, -10976, -11200, 10816, 9696, -6464, 7680, -9536, 10688, 4736, -3424,
7616, 2656, -10432, 9504, 9856, 8608, 7040, -2528, -9248, -3232, 5952, 3744, -1952,
5888, -9696, -7840, -1920, -5056, 5536, -704, 2080, -544, 6560, -9344, 6464, -3680, 4032, -3552, 672,
8544, -3488, 7808, -8704, 2880, 7712, -7904, 4320, -3520, -6912, -768, -8320, 3232, 672, 2176, -5920, 6112,
1120, 5664, 224, -7744, -8000, -1504, -6752, 992, 5504, -2848, -448, -928, -7424, 3360, -3168, 512, 7232,
768, -7040, 0], "i_remote": [0, 0, 0, 0, -7808, -7616, 7744, 7296, -5536, 4192, -5792, 7360, 3616, -2720,
4832, 2720, -6976, 6528, 6464, 5408, 4640, -1344, -6304, -1504, 4192, 2816, -832,
3872, -6112, -5248, -1024, -3680, 3776, -736, 992, -800, 4512, -6112, 3616, -2048, 3360, -2688, 1024,
5344, -1824, 4640, -5440, 1504, 4736, -5440, 2400, -1440, -3904, 224, -5440, 2560, -224, 768, -4512, 4512,
1504, 3008, -896, -5376, -4768, -2176, -3872, -544, 2528, -544, -1376, -1728, -4544, 3616, -576, 2112, 4928,
2304, -4128, 0], "q_remote": [0, 0, 0, 0, -320, -1568, -288, -2496, 5408, 6400, -4960, -1632, -6496, 6816,
5376, -6592, -512, -2144, 1984, 3936, 4704, -6432, 1696, -6304, -4928, -5824, -6400, -5152, -1984,
3680, -6368, 5248, 5120, -6368, -6272, -6240, 4352, 1248, -5056, 5792, 5088, -5408, 5856, -2496,
5536, -3488, 1728, -5504, -3136, -1472, -5056, 5376, 3840, 5472, 576, 4864, -5504, -5472, -3136, 3104,
5248, -4544, -5376, -480, 2528, -4928, 3680, -5312, -4672, 5248, -5088, -4992, 2656, 3808, 5152,
4640, -1216, 4416, 2688, 0], "hopping_sequence": [30, 66, 56, 41, 22, 38, 20, 61, 37, 25, 35, 43, 36, 21,
42, 32, 17, 12, 59, 26, 54, 71, 50, 29, 55, 10, 73, 60, 64, 16, 48, 62, 52, 57, 46, 13, 40, 75, 72, 67, 19,
69, 14, 7, 53, 24, 11, 18, 58, 65, 45, 31, 78, 74, 34, 5, 15, 6, 63, 76, 68, 44, 47, 51, 33, 4, 77, 28, 8,
27, 23, 9, 39, 70, 49], "sinr_local": [0, 0, 0, 0, 0, 0, 0, 0, 0, 0, 0, 0, 0, 0, 0, 0, 0, 0, 0, 0, 0, 0, 0,
0, 0, 0, 0, 0, 0, 0, 0, 0, 0, 0, 0, 0, 0, 0, 0, 0, 0, 0, 0, 0, 0, 0, 0, 0, 0, 0, 0, 0, 0, 0, 0, 0, 0, 0,
0, 0, 0, 0, 0, 0, 0, 0, 0, 0, 0, 0, 0, 0, 0, 0, 0, 0, 0, 0, 0, 0, 0, 0, 0], "sinr_remote": [0, 0, 0, 0, 0, 0, 0, 0, 0,
0, 0, 0, 0, 0, 0, 0, 0, 0, 0, 0, 0, 0, 0, 0, 0, 0, 0, 0, 0, 0, 0, 0, 0, 0, 0, 0, 0, 0, 0, 0, 0, 0, 0, 0,
0, 0, 0, 0, 0, 0, 0, 0, 0, 0, 0, 0, 0, 0, 0, 0, 0, 0, 0, 0, 0, 0, 0, 0, 0, 0, 0, 0, 0, 0, 0, 0, 0, 0, 0],
"ifft[mm]": 166, "phase_slope[mm]": 247, "rssi_openspace[mm]": 398, "best[mm]": 166, "highprec[mm]": 155,
"link_loss[dB]": 32, "duration[us]": 20087, "rssi_local[dB]": 23, "rssi_remote[dB]": 26, "txpwr_local[dB]":
8, "txpwr_remote[dB]": 8, "quality": 0}

Figure 26: Example of a JSON file containing measurement results

6 Revision

6.1 Review of the measurement method

Before the theoretical model can be revised, a second look at the hardware is necessary. This includes a re-examination of the measurement method as well.
The measured data is stored on the computer in a JSON file. Figure 26 shows an example of such a JSON file. Notice the four data sets, namely *i_local*, *q_local*, *i_remote* and *q_remote*. These data sets contain the I and Q values at the initiator and at the reflector for the different frequency channels. From these four data sets, it can be deduced that the transfer function is measured twice. Once at the initiator and once at the reflector. Instead of having one transfer function which travels twice through the channel, there are now two transfer functions measured. One from initiator to reflector and one from reflector to initiator.
The *hopping sequence* contains the unique sequence by which the frequency channels are used in the measurements. Notice that there are more than 40 frequency channels used.

[19] explains the measurement method in more detail. Using the I and Q values, the transfer function of the channel can be reconstructed at the initiator and at the reflector. The reflector does not match its LO to the initiator. To compensate for this the transfer function of the channel was measured at the initiator and at the reflector. These two measured transfer functions only contain the channel in one direction. Now there is an extra phase shift θ present in the equations, corresponding to the phase difference between the LO of the initiator and the reflector.

$$\begin{aligned} X_i + jY_i &= A_r|H(f_k)|e^{j\phi} * e^{j\theta} \\ X_r + jY_r &= A_i|H(f_k)|e^{j\phi} * e^{-j\theta} \end{aligned} \tag{24}$$

A_r and A_i represent the magnitudes at which the signals at the reflector and the initiator respectively were transmitted. Since the transfer function is measured at both antennas, the phase shift θ has the opposite sign for both equations.
The transfer function of the channel can now be calculated by multiplying both equations. This will negate the phase difference introduced by the LO's. Since the channel is considered to be symmetrical, the equation will look as follows.

$$(X_i + jY_i) * (X_r + jY_r) = A^2|H(f_k)|^2 e^{j2\phi} \tag{25}$$

There is also noise present in the channel and the hardware. The following equation shows the influence the noise has on the transfer function:

$$(X_i + jY_i + n_i) * (X_r + jY_r + n_r) = H(f_k)^2 + H(f_k)(n_i + n_r) + n \tag{26}$$

Now, however, signal dependent noise is present in the equation. This makes it more difficult and less accurate to derive the transfer function.

Another big difference is that the frequency channel width is $1MHz$ instead of $2MHz$. This lowers the resolution to $1.875m$ instead of $3.75m$.
Now there are 80 frequency channels inside the range from $2.4GHz$ to $2.480GHz$. Furthermore, the first frequency channel used is the $2.402GHz$ one and not $2.4GHz$. Now the last frequency channel has center frequency $2.480GHz$ and not $2.478GHz$.
When looking at the JSON file in figure 26, the first four measurements and the last measurement are all 0. The hopping sequence only contains 75 frequency channels as well, with the lowest and highest frequency channels, channel number 4 and 78 respectively. From this, it can be concluded that frequency channels 0 through 3 and channel 79 are not used in the measurement method.

6.2 New theoretical model

In this part, a new theoretical model will be devised compatible with the above described measurement method.

While writing this thesis, no method to eliminate the LO offset θ was available yet. To find the channel transfer function, without signal dependent noise present, a different method needs to be used to eliminate this offset.
From both equations in 24, the phase can be isolated using the *phase* function in matlab. Of the noise present in the equations, only the phase part remains as well. The next step is to multiply these two phase parts with each other. This eliminates the phase shift θ from the equation. The resulting phase can be divided by two and unwrapped to obtain the true phase. There is still some noise present in this phase, but the noise is not signal dependent anymore.

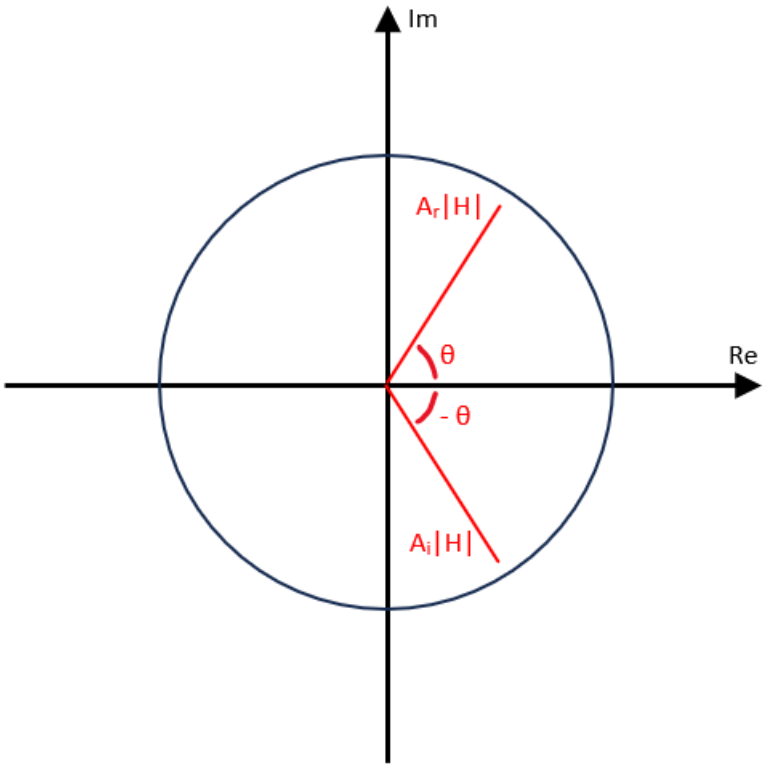

Figure 27: Magnitudes for both transfer functions visualized in the complex domain

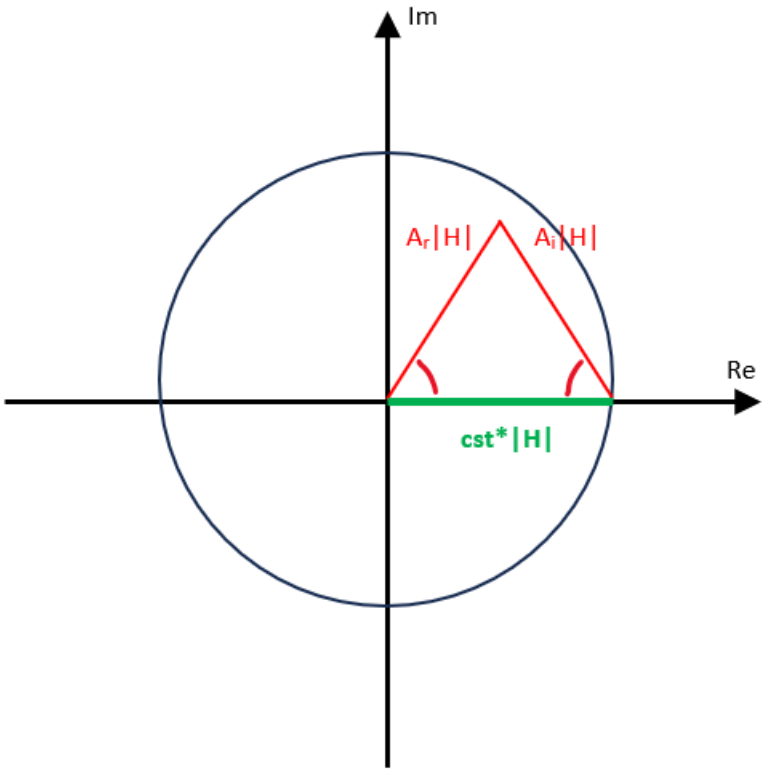

Figure 28: Sum of the magnitudes for both transfer functions

After obtaining the true phase, the equations in 24 can be multiplied with the inverse of this phase. This cancels out the phase part of the transfer function.
Since the value for θ is constant, only a scaling of the transfer function magnitudes remains.

$$\begin{aligned}(X_i + jY_i) * e^{-j\phi} &= A_r|H(f_k)| * e^{j\theta} \\ (X_r + jY_r) * e^{-j\phi} &= A_i|H(f_k)| * e^{j\theta}\end{aligned} \tag{27}$$

Figure 27 shows the equations in 27 in the complex domain. The channel is considered to be symmetrical, which means that $A_r|H|$ and $A_i|H|$ are equal. The phase offset θ can be eliminated by summing both parts as shown in figure 28. The resulting value can now be described as a constant belonging to the set of real numbers, multiplied with the transfer function magnitude. The small complex contributors originating from the noise, can be neglected.
The location of the peak in the IFFT of the transfer function is not influenced by the scaling of the transfer function. For the different path magnitudes, it is the ratio of reflected path magnitude to LoS path magnitude that contains the necessary information. This means that a scaling of the transfer function magnitude is sufficient information.

Multiplying the scaled version of the transfer function with the isolated phase will return a scaled estimate of the transfer function. This new transfer function can replace equation 10. Now the LSE algorithm can be used again to analyze the new estimated transfer function.

6.3 New Simulations

The same two situations as in section 4.2 will be simulated. This means that in the first situation, the LoS path is $5m$ long and the reflected path $15m$. In the second situation, the LoS path is $5.1m$ long and the reflected path $6.1m$, similar to the real life scenarios.

Figures 29 and 30 show the IFFT and the magnitude estimation for the scenario with a big difference in path lengths respectively.
The IFFT is highly innacurate and does not match the expected form at all. The path lengths that can be derived from this IFFT are $20.74m$ and $53.34m$.
For the estimated magnitudes, the reflected path magnitude is bigger than the LoS path magnitude. This should be physically impossible.

Figures 31 and 32 show the IFFT and the magnitude estimation for the scenario with a small difference in path lengths respectively.
Again the IFFT of the transfer function is highly innacurate. The estimated path lengths that correspond with the the peaks and their τ values, are $8.57m$ and $32.47m$.
For the estimated magnitudes, the reflected path magnitude is again bigger than the LoS path magnitude.

Consider the isolated phase from the equations in 27. This phase is shown in figure 33 and 34. In blue the expected phase is shown while the truly isolated phase is represented by the orange curve. The expected phase is linearly decreasing, while the truly isolated phase increases exponentially. This is best visualized in figure 34.

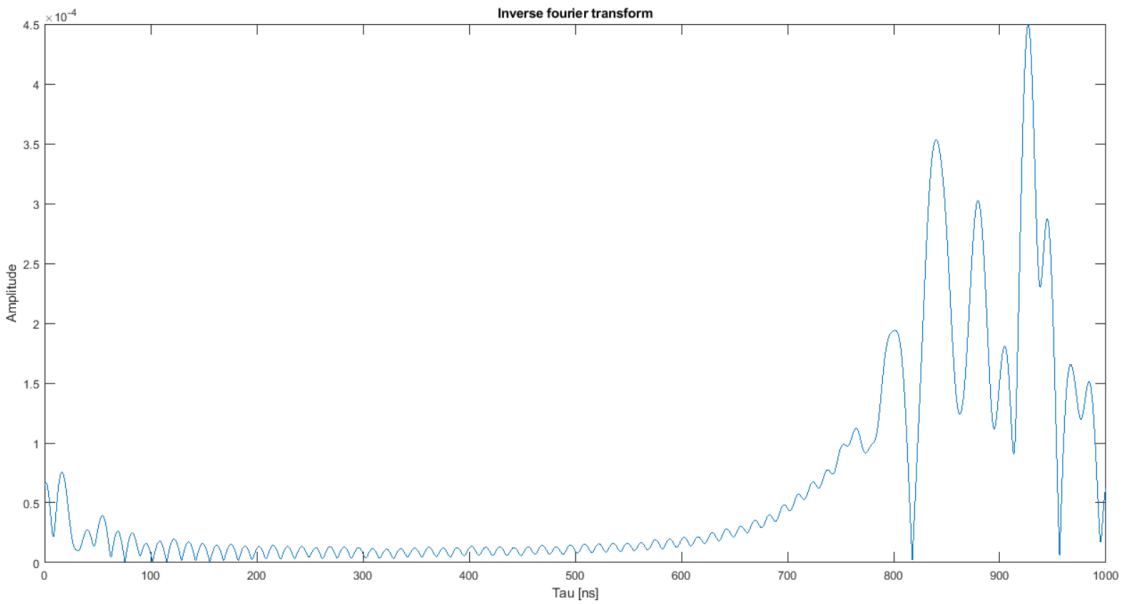

Figure 29: IFFT of the revised theoretical model for path lengths $5m$ and $15m$

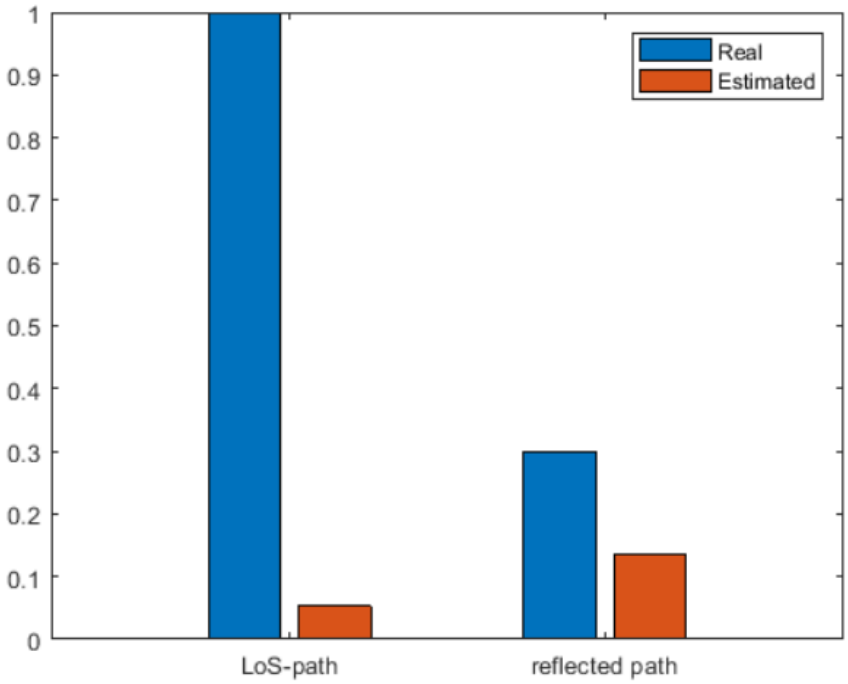

Figure 30: Magnitude estimation of the revised theoretical model for path lengths $5m$ and $15m$

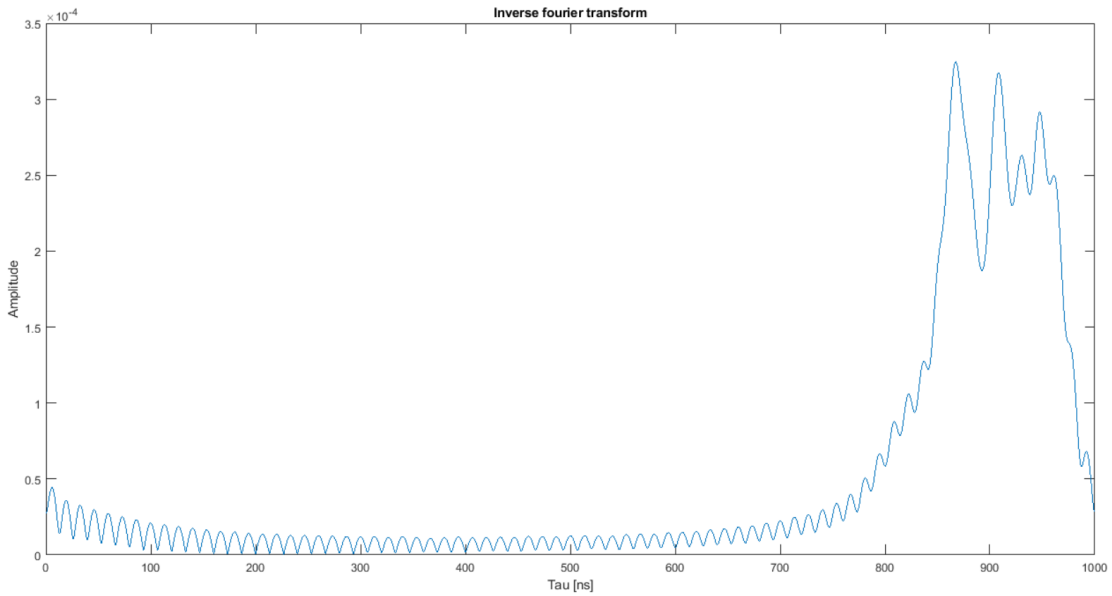

Figure 31: IFFT of the revised theoretical model for path lengths $5.1m$ and $6.1m$

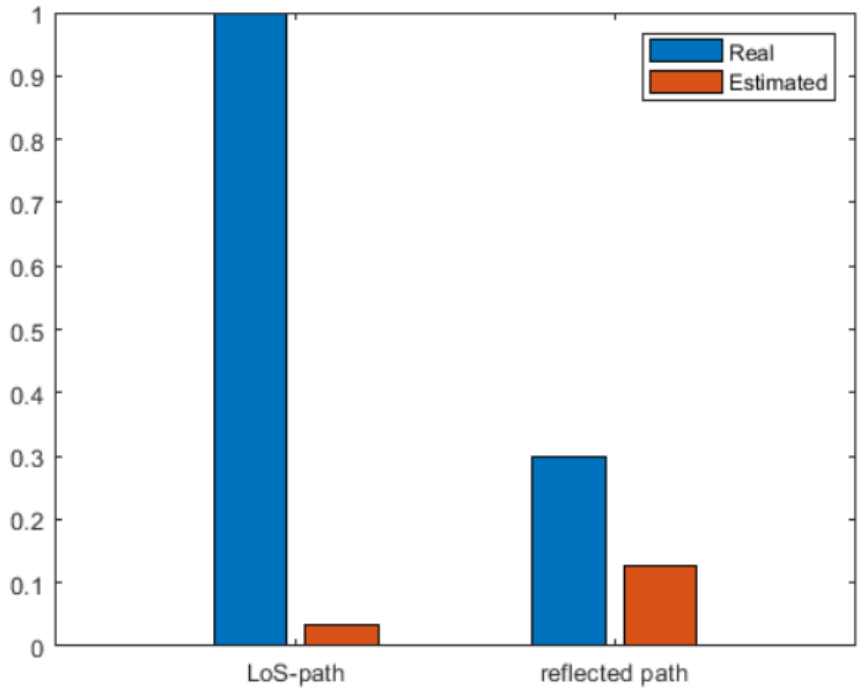

Figure 32: Magnitude estimation of the revised theoretical model for path lengths $5m$ and $15m$

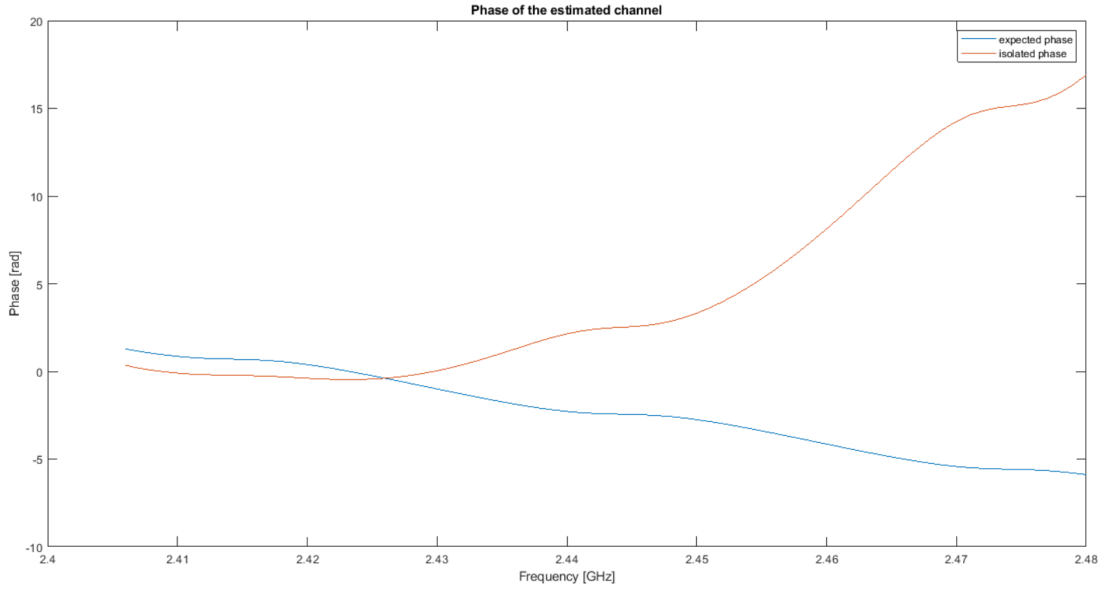

Figure 33: Isolated phase compared to the expected phase for path lengths $5m$ and $15m$

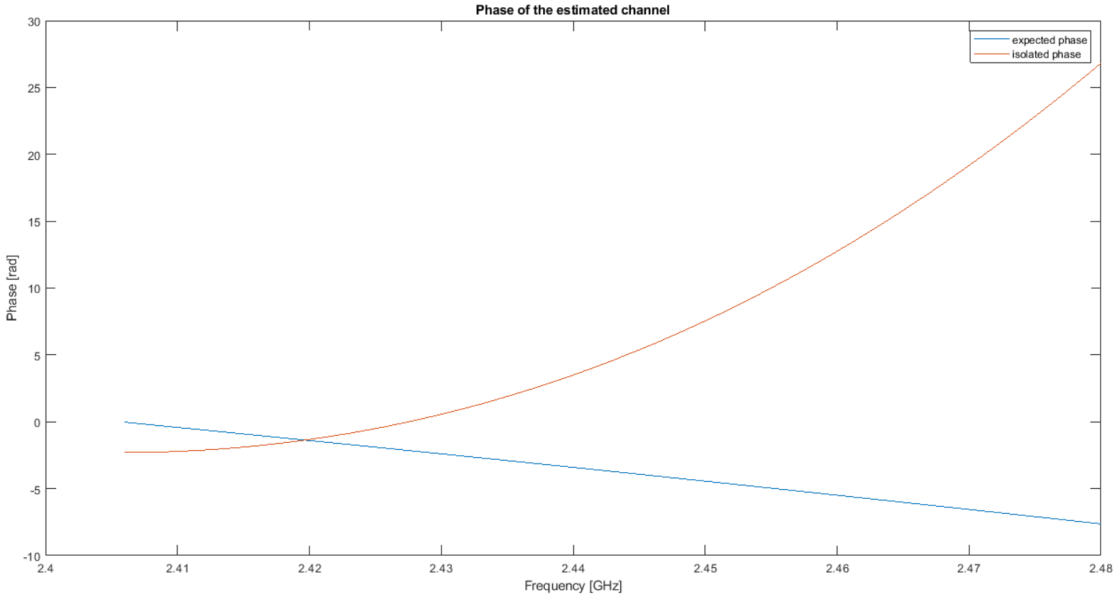

Figure 34: Isolated phase compared to the expected phase for path lengths $5.1m$ and $6.1m$

Table 5: Overview of the analyzed situations with signal dependent noise present

Situation	Type of path	τ [ns]	Estimated length [m]	Magnitude ratio
1	LoS	8.8762	2.6628	0.8410
	Reflected	46.1536	13.8461	
2	LoS	5.6455	1.6936	0.6436
	Reflected	27.1582	8.1475	

This insinuates the presence of frequency dependent noise. More specific, an exponentially increasing frequency dependent noise.
The proposed method to estimate the phase shift introduced by the channel, is flawed. The simulations can be tried using the phase isolated from equation 25 as well. Of course this means that signal dependent noise will be present in the estimation, making it less accurate.

Figure 35 shows the IFFT of the channel transfer function for path lengths $5m$ and $15m$. In table 5 this is represented by situation 1. Figure 36 shows the corresponding path magnitude estimation for this situation.
Situation 2 represents the data corresponding to path lengths $5.1m$ and $6.1m$. Here figure 37 shows the IFFT of the channel transfer function and figure 38 shows the path magnitude estimation.

The form of the transfer function is more in line with the expected form. There is a peak located at a small τ value. This corresponds to the LoS path. Using the *rootmusic* algorithm, the τ corresponding with the reflected path can be found. The smaller peak located at this secondary τ is not visible, since the path length difference is smaller than the resolution.
The calculated path lengths are not accurate. This is to be expected since there is signal dependent noise present in the estimation.
however, the estimated lengths vary around the expected values. Taking into account the great amount of present noise, the estimated path lengths match the expected path lengths.

The path length estimation is inaccurate due to the inaccurate phase used in the estimation. However, it can be concluded that, despite the present noise, the new method to estimate the transfer function magnitude is a valid and proper method. If now the transfer function phase can be isolated accurately, a correct theoretical model of the transfer function can devised.

The ratio of estimated magnitudes still does not meet the expected ratio. It can be concluded that the theoretical part in section 3.2 needs to be adjusted for the magnitude estimation to be correct.

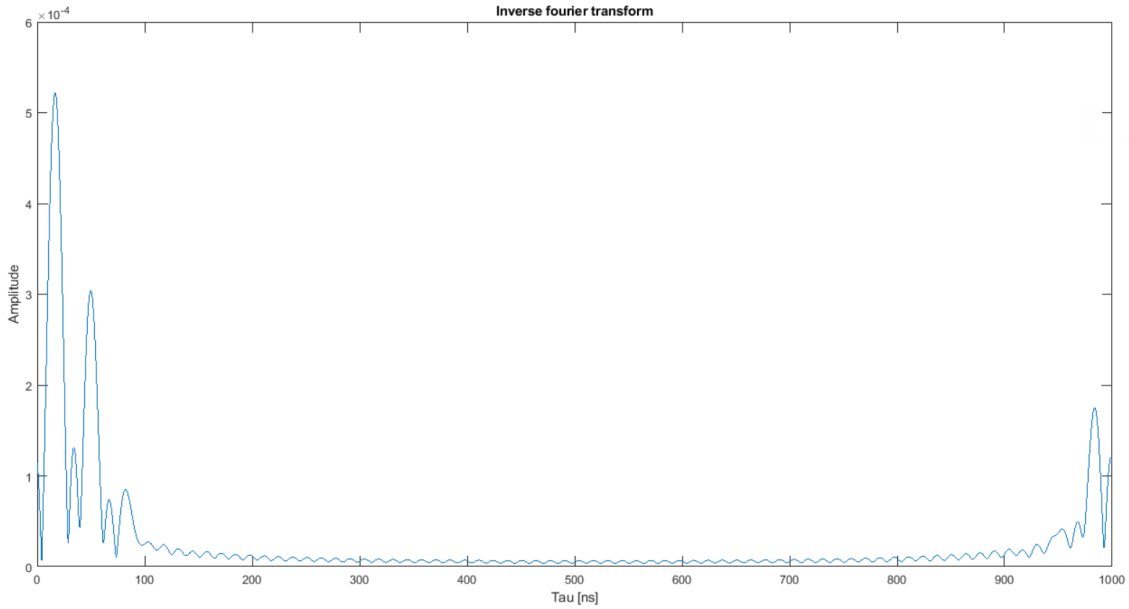

Figure 35: IFFT of the revised theoretical model for path lengths $5m$ and $15m$, signal dependent noise present

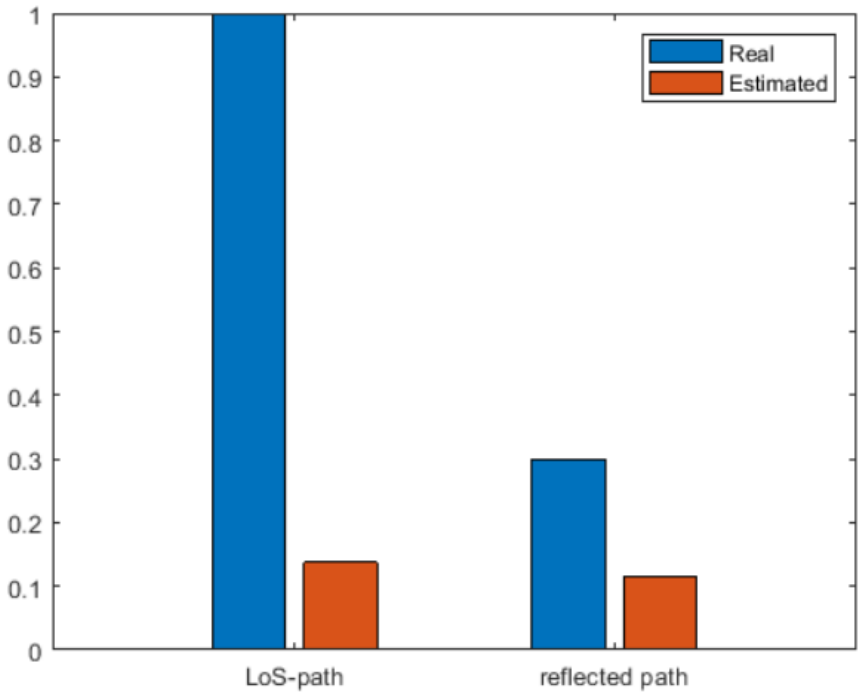

Figure 36: Magnitude estimation of the revised theoretical model for path lengths $5m$ and $15m$, signal dependent noise present

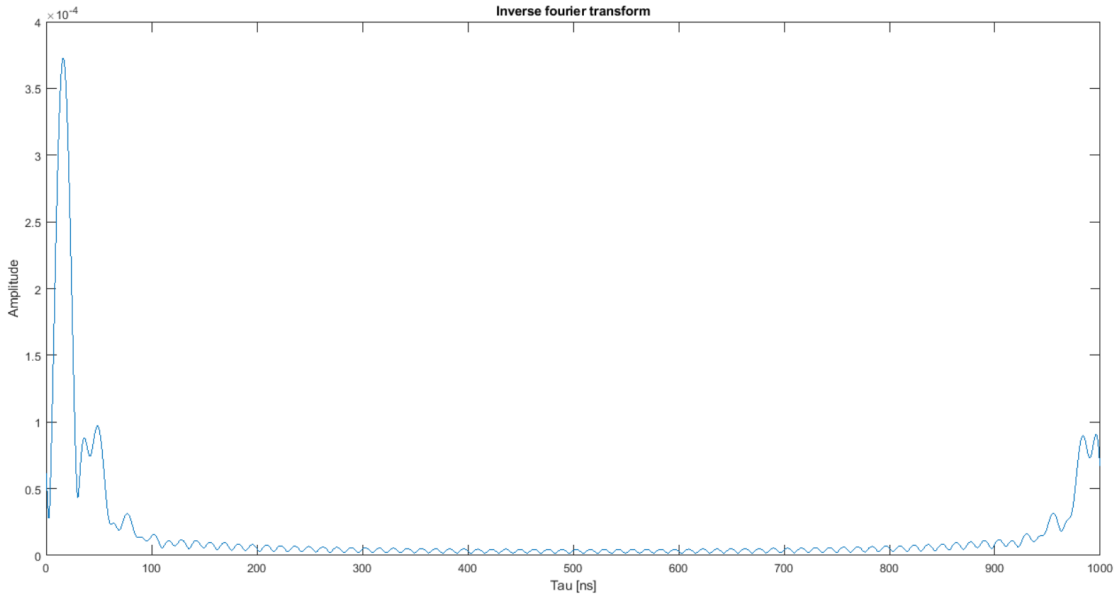

Figure 37: IFFT of the revised theoretical model for path lengths $5.1m$ and $6.1m$, signal dependent noise present

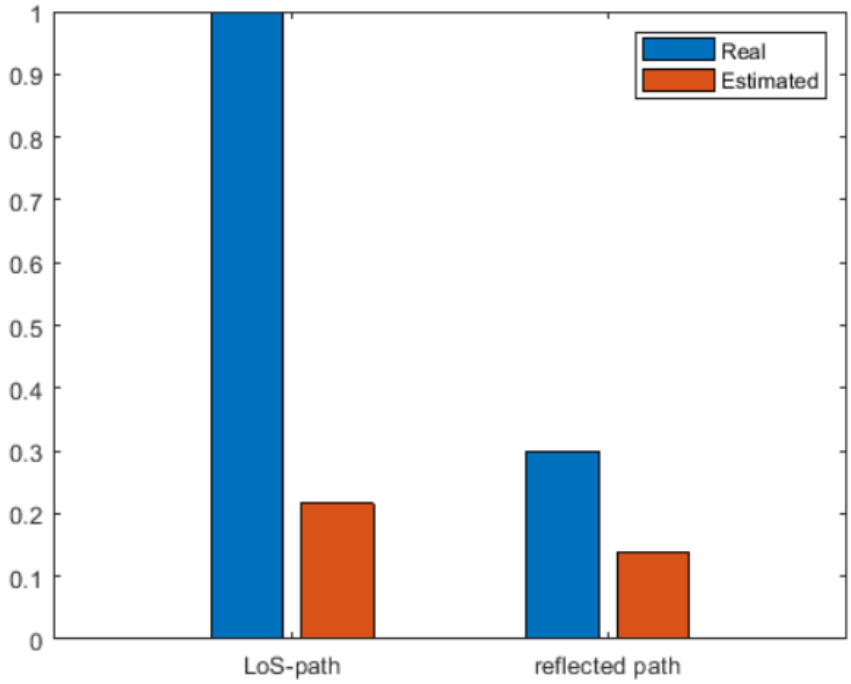

Figure 38: Magnitude estimation of the revised theoretical model for path lengths $5.1m$ and $6.1m$, signal dependent noise present

7 Conclusion

In this thesis, the multipath channel between two antennas was investigated. Since this research acts as a starting point, the multipath only contains 2 paths. A theoretical model was devised and presented to represent this multipath channel. Simulations for this theoretical model showed promising results for the path length estimations with low noise levels. For an SNR equal to $60dB$, the relative error on the estimated path lengths was smaller than 0.1% for a $10m$ difference in path length and smaller than 0.6% for a $1m$ difference in path length. The magnitude estimations however were not accurate.
Following this, a multipath environment using two antennas and one reflecting object was created in an anechoic chamber. This ensures that the multipath consists of only two paths. The measurements from this setup, did not support the theoretical model. The calculated path lengths were more in line with half the expected values.

A second and more thorough examination of the hardware and measurement method was necessary. Because a specific type of hardware is used in this research, the presented theoretical model needs to match this hardware. This means that the first theoretical model can be a correct model provided that the hardware used, matches the assumed measurement method. However, that is not the case in this thesis.
After analyzing the measurement method and the used hardware, the existence of an extra phase shift caused by a phase offset between the LO of the antennas was detected. A new theoretical model was presented taking into account this extra phase shift.
To create this model, first the channel phase shift was isolated. This way, the signal dependent noise present can be eliminated. Next, the complex values are eliminated from the channel magnitude, leaving only a scaled version of the magnitude. The simulations imply that there is frequency dependent noise present in the isolated phase. The theoretical model was simulated with the signal dependent noise to test the channel magnitude estimation part of the model. The estimated path lengths match the expected values despite having a large error due to the signal dependent noise. This concludes that the channel magnitude can be estimated as presented in the theoretical model.

The estimated path magnitudes never have the expected ratio. Despite the large influence of present noise, the estimated path lengths still match the expected values. Since the path magnitudes and path lengths together form the function describing the path, it is peculiar that the path magnitude estimation does not match the expected values. Even with a big influence of the present noise.
This insinuates that method for analyzing the theoretical model for the multipath channel, needs to be adjusted.

The following steps in this research are to adjust the LSE to analyze the theoretical model, so that the path magnitude estimation matches the expected values.
It is also important to find a good way to isolate the phase shift introduced by the channel. This way, the signal dependent noise can be eliminated from the estimation.
Once the theoretical model meets these requirements and matches the measurements, the integration of a Bluetooth connection is necessary. This allows to expand the theoretical model to situations with more than two antennas.

For the case where there are more than two paths present in the multipath, it is hypothesized that the completed version of the theoretical model presented in this research will be able to estimate this as well.

The addition of paths and antennas is a crucial step in further research. Since the proposed practical utilizations and all other possible utilizations will need a system consisting of a lot more antennas than two.
For the utilizations in which the environment needs to be mapped, the multipath will consist of a lot more paths than two as well.

8 Acknowledgement

I am deeply grateful to all those who provided support for the research presented in this thesis. In particular to my supervisors Prof. dr. Torbjörn Ekman and Prof. dr. ir. Jo Verhaevert for their continuous support, insights and advice regarding this research.
Also, I am grateful to my co-supervisor Carsten Wulff for his advice regarding the hardware, as well as Jenny Aune Forbord and Johan Suarez for their support with the hardware setup configuration.
To close, I would like to show my gratitude towards Prof. dr. Herman Van den Broeck and my father Luk Hendrickx for proofreading this thesis.

References

[1] TeraSense. *Radio Frequency Bands*. 2023. URL: https://terasense.com/terahertz-technology/radio-frequency-bands/ (visited on 15th June 2023).

[2] Nordic Semiconductor. *nRF52833 DK*. 2023. URL: https://www.farnell.com/datasheets/2865878.pdf (visited on 5th July 2023).

[3] N. Augustine. *Internal Antennas: Different Types and Advantages*. 2021. URL: https://www.symmetryelectronics.com/blog/internal-antennas-different-types-and-advantages-symmetry-blog/ (visited on 5th July 2023).

[4] P. Zand et al. 'A high-accuracy phase-based ranging solution with Bluetooth Low Energy (BLE)'. In: *2019 IEEE wireless communications and networking conference (WCNC)*. IEEE. 2019, pp. 1–8.

[5] M. Pelka, C. Bollmeyer and H. Hellbrück. 'Accurate radio distance estimation by phase measurements with multiple frequencies'. In: *2014 International Conference on Indoor Positioning and Indoor Navigation (IPIN)*. IEEE. 2014, pp. 142–151.

[6] P. Boer et al. 'Performance of high-accuracy phase-based ranging in multipath environments'. In: *2020 IEEE 91st Vehicular Technology Conference (VTC2020-Spring)*. IEEE. 2020, pp. 1–5.

[7] S. N. Shoudha et al. 'Reduced-Complexity Decimeter-Level Bluetooth Ranging in Multipath Environments'. In: *IEEE Access* 10 (2022), pp. 38335–38350.

[8] B. Everitt and D. C. Howell. 'Encyclopedia of statistics in behavioral science'. In: (2005).

[9] kiran086472. *Hermitian matrix*. 2023. URL: https://www.geeksforgeeks.org/hermitian-matrix/ (visited on 10th June 2023).

[10] P. Zand et al. 'A high-accuracy concurrent phase-based ranging for large-scale dense BLE network'. In: *2019 IEEE 30th Annual International Symposium on Personal, Indoor and Mobile Radio Communications (PIMRC)*. 2019, pp. 1–7. DOI: 10.1109/PIMRC.2019.8904093.

[11] United Nations. *History*. 2023. URL: https://sdgs.un.org/goals#history (visited on 10th July 2023).

[12] United Nations. *Sustainable Development Goals*. 2023. URL: https://www.un.org/sustainabledevelopment/ (visited on 9th July 2023).

[13] J. Papiewski. *How to calculate the phase shift*. 2018. URL: https://sciencing.com/calculate-phase-angles-5972010.html (visited on 20th Mar. 2023).

[14] V. K. Garg. 'CHAPTER 3 - Radio Propagation and Propagation Path-Loss Models'. In: *Wireless Communications Networking*. Ed. by V. K. Garg. The Morgan Kaufmann Series in Networking. Burlington: Morgan Kaufmann, 2007, pp. 47–84. DOI: https://doi.org/10.1016/B978-012373580-5/50037-5. URL: https://www.sciencedirect.com/science/article/pii/B9780123735805500375.

[15] National Instruments. *Resolution bandwidth*. 2023. URL: https://www.ni.com/docs/en-US/bundle/ni-rfsa/page/nirfsa/resolution-bandwidth.html (visited on 22nd June 2023).

[16] Siemens. *Digital Signal Processing: Sampling Rates, Bandwidth, Spectral Lines, and more...* 2023. URL: https://community.sw.siemens.com/s/article/digital-signal-processing-sampling-rates-bandwidth-spectral-lines-and-more (visited on 22nd June 2023).

[17] Nordic Semiconductor. *Welcome to the nRF Connect SDK!* 2023. URL: https://developer.nordicsemi.com/nRF_Connect_SDK/doc/latest/nrf/index.html (visited on 5th June 2023).

[18] C. Wulff. *Nordic distance toolbox example [Source code].* 2023. URL: https://github.com/wulffern/nrfdmiq (visited on 8th June 2023).

[19] Core Specification Working Group. *Channel sounding*. 2023. URL: https://www.bluetooth.com/specifications/specs/channel-sounding/ (visited on 22nd June 2023).

A Git repository

The following Git repository contains the matlab codes used to simulate and analyze the theoretical models proposed in this thesis.

https://github.ugent.be/rubhendr/Thesis_MultipathChannelEstimation